UNIVERSITÀ
DEGLI STUDI
DI PADOVA

UNIVERSITA' DEGLI STUDI DI PADOVA

Dipartimento di Ingegneria Industriale DII

Corso di Laurea Magistrale in Ingegneria Aerospaziale

Estimating the decay rates of orbital debris through upper-atmosphere density data supplemented with on-board accelerometer measurements

Relatore: Prof. Enrico Lorenzini

Studente:

Daniele Scelsa 1110851

Anno Accademico 2018/2019

Abstract

One of the non-gravitational perturbative forces, acting on a satellite in LEO orbit, is the atmospheric drag that depends on the atmospheric density. This parameter is a particularly difficult to evaluate a priori, hence, towards the end of the last century, mathematical models were developed to estimate it. Because the model can't totally agree with reality, a percentage of error is always introduced when the propagation of an orbit is carried out. However, during the last years some satellites were launched with accelerometers on-board. Measurements of acceleration in-situ, after the modelling of non-gravitational forces (e.g. solar radiation pressure) acting on the satellites, allow to extract the drag acceleration and, knowing geometry and optical properties of satellite, it's possible to estimate the density.

The thesis focuses on the computation of density using both a mathematic model, MSISE-90, and accelerations measured by accelerometer of GRACE, satellite that was in orbit between 2002 and 2018 at 500 km of altitude. A comparison between the estimated density obtained from model and from the flying data is provided. Finally, the atmospheric density that could be provided by the proposed satellite METRIC is presented. This satellite has a 450-1200 km of altitude Sun-synchronous dawn-dusk orbit and, at the apogee, it could estimate directly the acceleration due to solar radiation pressure and therefore potentially leads to a better estimate of drag deceleration.

Summary

List of figures

List of tables

Introduction

Estimate of satellites life is one of the main challenges for designers because of the rough spatial environment, the possibility of a sudden collision with debris and the use of mathematical models for the computation of density that have errors due to the lack of experimental data. The consequence is that if satellites stay in their orbits for longer than it was valued, the altitude region has a higher density of debris, if they stay for less time, there is an economic and scientific loss. In both cases there are problems due to the presence of an element which could be possible debris or obstacle for other spacecrafts. In particular, changes in density create variations in the drag effects on the Low-Earth Orbits (LEO) and these effects must be carefully accounted for in LEO mission predictions.

The goal of this thesis is to calculate atmospheric density from accelerometers data to confront it with one got from the Mass Spectrometer - Incoherent Scatter 90 model (MSISE-90), that is older than NRLMSISE-00 but more precise, under some conditions, and to point out the differences between the two approaches. The availability of data from accelerometers onboard LEO missions offers great potential for the improvement of such density modeling efforts. Actually, there aren't many satellites that have accurate accelerometers on board, one of them is Gravity Recovery and Climate Experiment (GRACE), an Earth-gravity mapping mission launched in March 2002 and finished in March 2018, with twin satellites in 89 deg inclination, coplanar, 500 km alt orbits, separated by 220 km along the track- Each of the spacecrafts carried a superSTAR accelerometer having a sensitivity of 10^{-9} m/s^2. It allows to measure non-gravitational forces acting on the satellites, such as solar radiation pressure, air drag and attitude control actuators.

Starting from the accelerations measured by STARs and removing any bias and scale factor offsets, the contributions due to solar, albedo and infrared pressures will be subtracted to obtain accelerations caused only by air drag and the atmospheric density will be deducted. Values obtained have anyway an error due to drag coefficient, which is calculated by a mathematical model, geometry approximations, neglecting of the neutral winds and errors that build up with truncation and round-off due to fixed computer word length.

Afterwards, this procedure will be used for METRIC (Measurement of EnvironmenTal and Relativistic In-orbit preCessions), a proposed satellite that has, among its mission objectives, that of measuring accelerations to estimate the atmospheric density in the orbital region of interest.

Chapter 1

Density's mathematical models

The atmospheric density is one of the most important parameters to calculate drag deceleration and the most difficult to estimate with high accuracy. Currently, model atmospheres are the most used ways to calculate atmospheric density. Properties and development of these models are described in this chapter.

1.1. Density influencing factors

The density of the upper atmosphere changes because of a complex interaction between three fundamental parameters: the atmosphere's molecular structure, the incident solar flux of radiation and particles and geomagnetic interactions.

The atmospheric models can be static or time-varying. Of course, the firsts are simpler because they consider all the atmospheric parameters constant. The factors that affect them are: latitude, longitude and the altitude from Earth surface; hence, it's influenced by the planet's orography.

For time-varying models, there is a major complexity because additional effects are considered [23]:

- Diurnal variations: due to Earth rotation. A density maximum doesn't coincide with the direction of the Sun, where the atmosphere is warmest. The atmospheric bulge centers on the equator at the equinoxes but moves to higher latitudes depending on the Sun's declination, which varies throughout the year. So, the atmospheric density depends also on local time and the time of year.
- 27- day solar rotation cycle: due to Sun's rotational period and it causes a fluctuation which is correlated with the solar decametric-wavelength radio flux.
- 11-year cycle of Sun spots: it can vary seriously the amount of Earth's incoming solar radiation flux.
- Semi-annual/ seasonal variations: they last about six months and depend on the distance between Earth and Sun and the Sun's declination during the year.
- Cyclical variations: these variations cause a cycle that lasts as the cycle of the Sun spot but it's a few years late. The minimum of this cycle isn't in mid-term and the maximum of each cycle varies. The cause is unknown, but it's still linked to sunspot activity.

- Rotating atmosphere: the rotation of the atmosphere with the Earth causes extra time-varying changes in the density.
- Winds: they cause temperature variations and consequently changes in density.
- Magnetic-storm variations: variations of Earth's magnetic field cause alterations in atmosphere (and density), but effects can be larger when geomagnetic activity increases.
- Irregular short periodic variations: they include random solar flares and other small effects, as variation in hydrogen into the atmosphere, and, for this reason, their effects are very small.
- Tides: ocean tides could cause very little changes in atmospheric density.

The time-varying models provide complete and more accurate data respect to the static ones, but they have computational requirements that might be too severe for some applications.

The development of both the static and time-varying atmospheric models relies on few basic hydrostatic principles which are used to model atmospheric effects [1]. The first one is the ideal-gas law which relates the absolute pressure, p_o, the mean molecular mass of all atmospheric constituents, M, the acceleration due to gravity, g_o, the universal constant, R, and the absolute temperature:

$$\rho = \frac{p_o M}{g_o R T} \tag{1-1}$$

The linkage with temperature is important because the Earth's rotation exposes the atmosphere to the Sun in different ways during the year and the resulting solar heating and cooling affect density, but also it causes big difficulties in developing an exact model for density. The second relation is the hydrostatic equation, which relates the change in pressure, Δp, to the density, gravity and change in altitude, Δh:

$$\Delta p = -\rho g \Delta h \tag{1-2}$$

1.1.1. Magnetic field models

The effect of the magnetic variations of the Earth and Sun must be taken into account when atmospheric density is calculated because they are related to fluctuations in atmospheric density. The Earth magnetic field has a measurable influence on satellite operations, too. The effect appears in four ways: the charged particles from any magnetic disturbances cause ionization in the upper atmosphere, thereby affecting the density and, subsequently, the drag; the charges on the particles can actually alter the attractive forces experienced by the satellite; the ionization interferes with satellite tracking and communication; and variations in the

magnetic field of the charged particles can interfere with onboard electromagnets that impose torque and carry out slow attitude maneuvers. The attractive force on the satellite is very small and is almost always ignored. But the effect of ionization on atmospheric density is noticeable.

The magnetic field's strength varies with the environment around the Earth's, and the mean magnetic field is usually modeled with a low degree-and-order spherical-harmonic expansion. Direct collisions of the solar wind and air particles interacting with the Earth's geomagnetic field heat the atmosphere. Geomagnetic activity must be measured to determine the heat generated. The commonly used geomagnetic planetary index, k_p, is a quasi-logarithmic, worldwide average of geomagnetic activity below the auroral zones. Twelve stations record values of k measured every three hours. Once latitude corrections are applied, the average k_p is formed. The quasi-logarithmic identifier is used because values range from low activity (k_p = 0.0) to extreme geomagnetic activity (k_p = 9.0) and are quoted to the nearest third of an integer. The geomagnetic planetary amplitude, a_p, is a linear equivalent of the k_p index, designed to minimize differences at 50° latitude. It's also known as the 3-hourly index because eight values of a_p are averaged to create the daily planetary amplitude, A_p. The effects of drag resulting from magnetic disturbances are noticeable for satellites at altitudes between 300 km and 1000 km.

Planetary geomagnetic indices (k_p and a_p) are compiled using measurements from twelve observatories which lie between 48° N and 63° S latitudes; three of these are in the United Kingdom, two in Canada, three in the USA, and the remaining four in New Zealand, Australia, Sweden, and Denmark. The most accepted compilation of the measurements from these observatories is from the Institut für Geophysik at Göttingen University, Germany. The daily planetary amplitude is in gamma units, where

$$1\ gamma = 10^{-9}\ Tesla = 10^{-9} kg \cdot s/m \tag{1-3}$$

The range of values for A_p is from 0 to 400; values greater than 100 are rare, and values of 10-20 are average. The daily planetary amplitude tends to follow the 11-year cycle of sunspots, although consistently large maxima of A_p usually occur in the declining phase of each 11-year cycle of $F_{10.7}$. There is also a secondary semi-annual cycle due to the variable position of the solar wind with respect to the Earth's magnetosphere. This cycle is just as variable and hard to predict as the sunspot cycle. Variations of A_p from the sunspot and semi-annual cycles are mainly due to solar flares, coronal holes, disappearing solar filaments, and the solar-wind environment near the Earth (Fraser-Smith, 1972; Nostrand, 1984) [23]. Intense geomagnetic activity at the auroral zones affects the shape of the atmosphere and makes atmospheric density depend on latitude.

1.1.2. Solar flux data

Sun's overall activity determines most effects on the atmosphere. Indeed, during periods of solar minima, the incoming radiation is less than normal and only slightly influences most satellite orbits; while, periods of solar maxima can produce large unpredictable perturbations in many satellites.

The contribution of solar flux to atmosphere density is mainly from incoming solar radiation. Solar flux (the Extreme Ultra-Violet, EUV, radiation that heats the upper atmosphere, F_{EUV}) is very difficult to measure at the Earth's surface because the atmosphere doesn't allow transmission of EUV radiation. However, scientists have determined that both EUV and incoming solar radiation with a wavelength of 10.7 cm, $F_{10.7}$, originate in the same layers of the Sun's chromosphere and corona. Because the Earth's atmosphere is transparent to the $F_{10.7}$ radiation, we can infer the F_{EUV} measurements from the Earth-based measurements of 10.7 cm-length radio waves. Regular measurements of $F_{10.7}$ exist from 1940. It's measured in solar flux units, SFU, where

$$1\ SFU = 10^{-22}\frac{watt}{m^2 Hz} \tag{1-4}$$

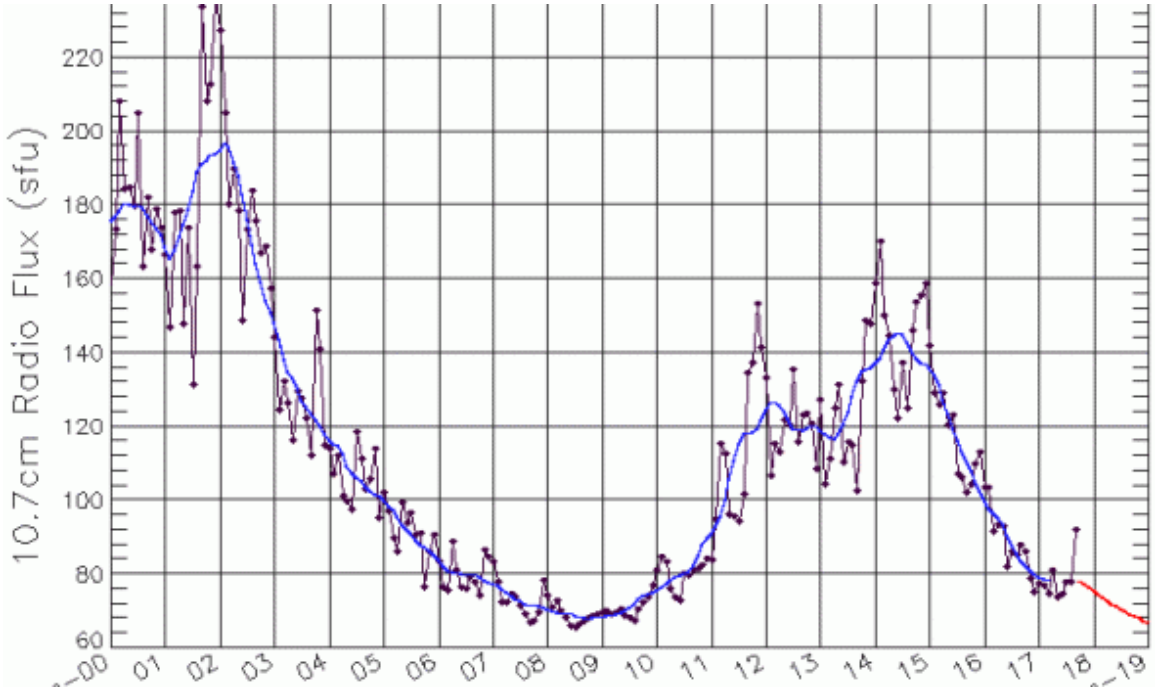

Figure 1.1: solar radio flux at 10.7 cm from 2000 to nowadays. Credit: NOAA

Typical values range from less than 70 to more than 300 SFU. The most commonly accepted measurement of $F_{10.7}$ is distributed daily by the National Oceanic and Atmospheric Administration (NOAA) at the National Geophysical Data Center in Boulder, Colorado.

Measurements are routinely made at the Algonquin Radio Observatory in Ottawa, Ontario, Canada. Monthly values are averaged to produce mean values denoted with a bar, $\bar{F}_{10.7}$.

In the past decades, scientists have seen that an inadequate EUV radiation proxy could be one of the main causes of atmospheric drag uncertainties [2][3]. So, an important number of studies and efforts were made to achieve new proxies more dependable. A possible result of this process is $E_{10.7}$, a new solar flux proxy, that is the integrated EUV energy flux spectrum between 1 and 105 nm ate the top of the atmosphere, reported in units of $F_{10.7}$. $E_{10.7}$ is designed to replace $F_{10.7}$, but it might also be an improvement of the knowledge of the energy input to the thermosphere and ionosphere. The $E_{10.7}$ values are available from the 14th February 1947 to a few weeks prior the present day. If it's necessary to have the nowcast values of $E_{10.7}$, they are available 24 hours prior of the current time, while the forecast values are provided from the present epoch to five solar cycles in the future.

An important issue about proxies is the accuracy of their measurements [1]. Indeed, each measurement has an uncertainty, that is never reported, and sometimes a value null is shown for the solar flux, but, obviously, this is a problem of the computation of the index. A possible way to have a value for these points is to do a linear interpolation between the adjacent points. This process provides a further error due to the interpolation, but it assures that it hasn't a zero input. Another complication linked to the accuracy issue is the use of observed or adjusted values for some of the parameters. The firsts are those values that are recorded directly and so they vary during the year due to the Earth's distance and orientation from the Sun, the others are the values that would be recorded at an average Earth-Sun distance. As it will be shown in the next paragraph, atmospheric density models use different values, for example Jacchia model uses the adjusted ones, while the MSIS models use the actual observed data.

$$F_{10.7(obs)} = \frac{F_{10.7(adj)} AU^2}{r_{\oplus-\odot}^2} \tag{1-5}$$

1.2. Models atmospheres

Several density models have been developed over the last decades of the last century from two main approaches: combining conservation laws and atmospheric-constituent models into a physical model and using simplified physical concepts developed from in-situ measurements and satellite-tracking data. Figure 1.2 shows the evolution of atmospheric models from 1960 to nowadays, the most important ones will be presented below.

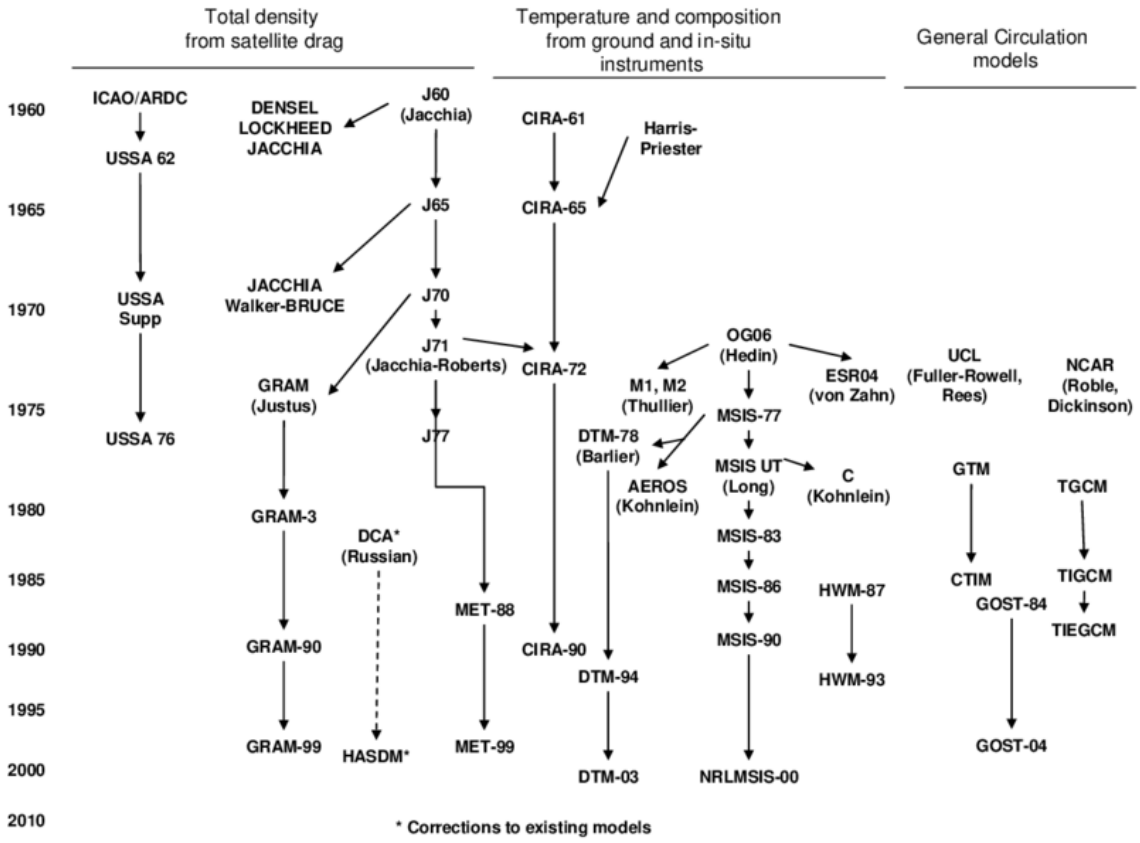

Figure 1.2: Evolution of density models from 1960 to 2010. The dashed line indicates that the concept for correcting the atmosphere followed the Russian work, but the models themselves are different. [1]

1.2.1.Jacchia-Roberts

The oldest models for atmospheric density and exospheric temperature are Jacchia ones, published in 1970 and revised in 1971 and 1977, but very popular yet in the operational orbit determination community [1]. The Jacchia-Roberts atmosphere contains analytical expressions for determining exospheric temperature as a function of position, time, solar and geomagnetic activity. With a computed temperature, we get density from empirically determined temperature profiles or from the diffusive equation.

Jacchia divided the upper atmosphere into two areas: 90-125 km and above 125 km. He determined this difference by assuming that the atmosphere is in a state of mixing between 90 and 100 km, with a fixed-boundary atmospheric condition at 90 km. In addition, Jacchia assumed diffusive equilibrium above 100 km, where the constituents N_2, O_2, O, Ar, He and H_2 are taken into account. This led to using a low-altitude temperature profile in the diffusion differential equation between 100 and 125 km and a high-altitude temperature profile above 125 km. Jacchia solved these differential equations by numerically integrating them over various constant values of exospheric temperature. The procedure uses an 81-day average of

solar parameters and, at first glance, this may seem arbitrary, but it's necessary to average out differences caused by the solar-rotation cycle (27 days), so we have a three-period cycle. Jacchia tabulated these results for use in atmospheric-drag simulations through interpolation. In 1971, Jacchia re-formulated his model using newer and more complete data. The changes are very important in comparison to the 1970 model. Finally, in 1977, the last Jacchia's revision includes satellite mass spectrometer data and a check of the equations from the previous models.

In 1971, Roberts recognized that tabular determination of atmospheric drag and numerical integration to calculate partial derivates for drag is computationally intensive. So, he analytically evaluated the 1970 Jacchia models. Roberts used fractions to integrate values between 90 and 125 km. For altitudes above 125 km, he introduced a different asymptotic function than the one Jacchia introduced to achieve an integrable form. With this substitution, Roberts closely approximates Jacchia's results above 125 km. Despite he made his corrections on the 1970 Jacchia model, it's possible to use them also for the following models [23].

During the developments of Jacchia model, sounding rockets and satellites were used.

Name	Norad #	Period	Incl.	Ap alt	Per alt	RCS	Launch/Decay
EXPLORER 17 (S-6)	564	87.9	57.6	186	151	N/A	03/04/1963 to 24/11/1966
EXPLORER 32 (AE-B)	2183	87.5	64.5	162	140	0.4954	25/05/1966 to 22/02/1985
ECHO 2 (A-12)	740	94.5	81.4	522	465	N/A	25/01/1964 to 06/07/1969
EXPLORER 19 (ADI-1)	714	90.1	78.7	301	259	13.7332	19/12/1963 to 10/05/1981
EXPLORER 8	60	94.8	49.9	664	353	0.5910	03/11/1960 to 28/03/2012
EXPLORER 1	4	88.5	33.1	215	183	N/A	01/02/1958 to 03/31/1970
INJUN 3	504	88.0	70.2	185	161	N/A	13/12/1962 to 25/08/1968

Table 1.1: satellites used to collect data for Jacchia model [1]

1.2.2. MSIS-86

In 1986, the Mass-Spectrometer-Incoherent-Scatter (MSIS-86) was developed by A. E. Hedin and his colleagues [4]. This is an empirical model of thermospheric temperature, density and composition that provides predictions of temperature and densities for He, O, N_2, O_2, Ar and H. It was developed from the MSIS-83 that was a sort of prototype for MSIS models and was based on in situ data from seven satellites (OGO 6, San Marco 3, AEROS-A, AE-C, AE-D, AE-E, ESRO 4) and some rocket probes, as well as five ground based incoherent scatter stations (Millstone Hill, St. Santin, Arecibo, Jicamarca, and Malvern). Between the 1983 and 1986, expecially, the in-situ composition measurements from the Neutral Atmosphere Composition Spectrometer (NACS) instrument and temperature ones from the Wind And Temperature Spectrometer (WATS) instrument of the Dynamics Explorer B (DE-B) satellite have become available, providing good coverage of the polar regions just after the peak of solar cycle 21. In addition to these data, the model includes new incoherent scatter temperature data from St. Santin and atomic nitrogen data from the AE-C, AE-D, AE-E and DE-B satellites. This updating allowed to better represent seasonal variations in the polar regions under both moderate and high magnetic activity, to introduce local time variations in the magnetic activity effect and to add a new specie, the atomic nitrogen.

The model uses a Bates temperature profile as a function of geopotential height for the upper atmosphere and an inverse polynomial in the geopotential height for the lower thermosphere. The temperature profiles allow exact integration of the hydrostatic equation (see eq 1-2) for a constant mass to determine a density profile based on a density specified at 120 km as a function of a geographical and solar/magnetic parameters. There is a smooth transition from mixing to diffusive equilibrium around 105 km. The density profiles for mixing conditions are calculated using the mean molecular weight for the lower atmosphere with the diffusive and mixing profiles equal at the turbopause.

The basic expansion formula used to express temperature and other parameters as a function of local time, geodetic latitude and longitude, Universal Time, solar F10.7 flux (for previous day and three-month average), magnetic A_p index (daily or A_p history for the last 59 hours) and, compared to the MSIS-83, terms that expressed hemispherical and seasonal differences in the polar regions and local time in the magnetic activity effect were added.

As it's possible to see in figure 1.3, the global and time averaged temperature profiles from MSIS-86 are within 1% of the MSIS-83 temperatures and the densities within 10%. The average exospheric temperature and total density at various solar activity levels are like MSIS-83 and within 10% of Jacchia77. The exospheric temperature and the density of all atmospheric species, except hydrogen and molecular oxygen increase with solar EUV radiation. At 120 km, the temperature enhances with $F_{10.7}$, in agreement with incoherent scatter, and also the

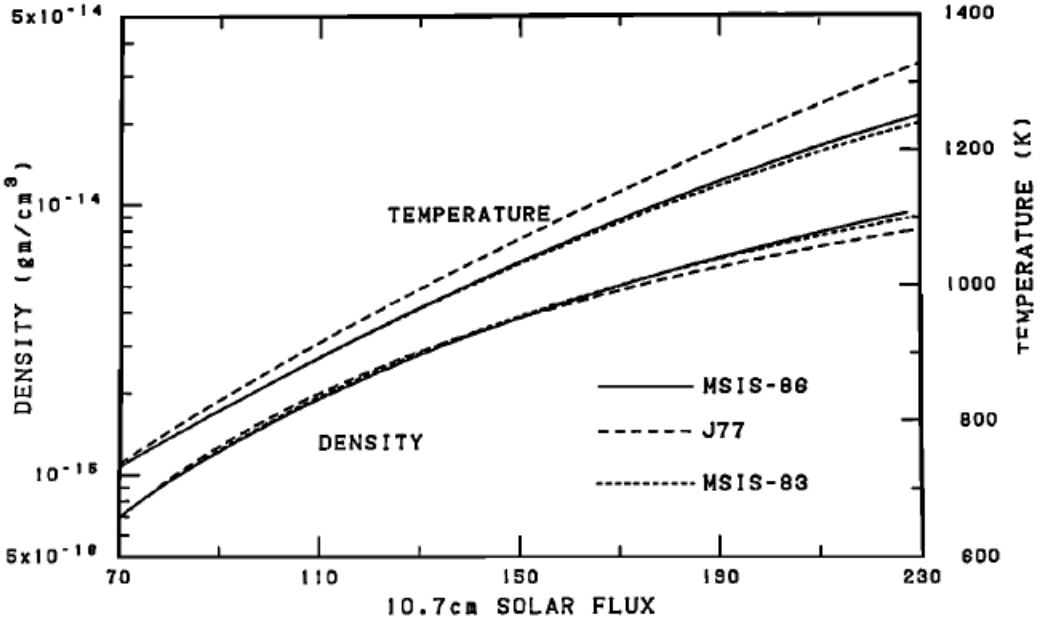

Figure 1.3: Average MSIS-86 total mass density and temperature at 400 km vs $F_{10.7}$ with the J-77 and MSIS-83 models shown for comparison [4]

temperature gradient increases, although the shape factor in the Bates temperature profile decreases with solar radiation, in agreement with incoherent scatter. Over the thermosphere, the temperature and density of some species (N_2, O_2 and Ar) increase towards the poles under magnetically quiet conditions, while the density of O, N, He and H decreases.

The temperature and species heavier than atomic oxygen have predominantly asymmetrical seasonal variations with summer maxima while the lighter species, except atomic nitrogen, have a winter maxima. Atomic oxygen, instead, has a winter maximum at lower altitudes and a summer maximum at higher altitudes. All the species have a significant semiannual variation, even if the species that have a predominant one, maximized near the equinoxes, are the atomic oxygen and molecular nitrogen. There is a 5 to 10% symmetrical annual variation, maximizing near the end of the year for all species except hydrogen, which when combined with the semiannual one brings to a principal minimum in July and a maximum in October at equatorial latitudes. The temperature and N_2 semiannual variations are quite stronger in the northern hemisphere than in the southern one, where, instead, the oxygen, helium and atomic nitrogen variations are higher. At higher latitudes the symmetrical annual component combined with the seasonal one leads to larger annual variations in He and O densities for the northern hemisphere.

In the high thermosphere, the variations are predominantly diurnal, with temperature and the heavier species maximizing near 16 hours local time, the atomic oxygen maximizes close to 14 hours local time, helium at 7 hours local time and hydrogen at 3 hours local time. The phase and amplitude of diurnal, semidiurnal and terdiurnal temperature variations depend on season

so that the temperature maximum is bigger in summer than in winter. Below 160 km the semidiurnal variation becomes predominant in density and temperature, whit peaks in the semidiurnal temperature amplitudes between 100 and 120 km.

Another element that affects a lot temperature and density profiles is the magnetic activity. In fact, if the magnetic activity increases from its state of quiet, both temperature and densities for all species, except hydrogen, increase. The main changes occur near the poles where temperature and neutral species heavier than atomic nitrogen increase with magnetic activity and lighter species decrease. Unlike MSIS-83, the greatest variations with magnetic activity occur near the winter pole, although the magnetic activity effects extend further toward the equator in summer so that at the mid-latitudes the largest effects are found in the summer consistent with incoherent scatter. Another new feature of the 1986 model is the maximum in magnetic activity effects in the midnight to early morning local time sector. As in MSIS-83, instead, there is an alternate representation of storm effects using the 3-hour A_p index to provide a more realistic description of the time history of an event. The time constants found for the decay in storm response after an impulse event range from 7 to 12 hours on average. However, in MSIS-86 a latitude variation of the storm response time was allowed and for He and exospheric temperature resulted in significant pole to equator increase in time constant of 2 and 4 hours, respectively.

The last terms which modify temperature and species' density are the longitude and the universal time. The longitude terms increase temperature and density for the heaviest species close to the magnetic poles, especially in winter, according to the DE data. As with other variations, the lighter species tend to decrease, particularly at lower altitudes, although atomic nitrogen is enhanced near the magnetic poles. The 24-hour universal time terms cause temperature peaks near 8.5 hours UT in the southern hemisphere, where the amplitudes are larger, and 20.5 hours in the northern. This variance adds a 24-hour variation to the magnetic polar increases and, combined with the longitude variations, results in enhancements in the early morning magnetic local time.

1.2.3. MSISE-90

The Mass-Spectrometer-Incoherent-Scatter (MSIS-90) is a revision of the MSIS-86 model conducted by Hedin and his colleagues [5]. The main goal of this model is to extend the MSIS-86 model into the middle and lower atmosphere because all the previous models had a lower-altitude limit near the mesopause for historical and measurements reasons. This necessity was due to the growing interest in understanding the coupling between atmospheric regions, and, consequently, it was convenient to have models which span atmospheric regions in a uniform way providing temperature, density and pressure profiles confirming to existing data as well

as possible. Zonal average tabulations from Middle Atmosphere Program (MAP) Handbook 16, proposed as the lower atmosphere portion of COSPAR International Reference Atmosphere (CIRA-86), were used to extend the previous model, along with rocket and incoherent scatter data in the upper mesosphere and lower thermosphere.

As in the MSIS-86 model, the present model uses the same temperature profiles for the upper, Bates exponential, and the lower thermosphere, inverse polynomial, which allow exact integration of the hydrostatic equation (see eq. 1-2) for a constant mass to determine the diffusive equilibrium density profile for each important species. The exospheric temperature and density of each species at 120 km are function of local time, latitude, longitude, UT, $F_{10.7}$, and A_p using spherical harmonics for latitude versus local time or longitude variations with Fourier series in time of day and day of year, and polynomials for variations with the $F_{10.7}$ index and A_p index. Well below the turbopause, which is near 105 km-alt, density profiles are calculated using the mean molecular weight of the lower atmosphere, assuming equality with diffusive profiles at the turbopause. The net density profile near the turbopause is a root mean of the diffusive and mixing profiles for a smooth transition. Initially, it was planned to extend the polynomial formulation of altitude profiles in the lower thermosphere by segmenting the atmosphere at the mesopause, near 85 km-alt, stratopause, between 50 and 55 km-alt, and tropopause, 12 km-alt on average, and harmonically expanding the height and temperature of these significant points. However, it was found that this formulation resulted in unacceptable nonlinear coupling between harmonics when temperature was integrated to determine density. Instead, a cubic spline formulation is used to calculate inverse temperature, inverse and not direct to facilitate integration for density computation, defined by cubic polynomials between specified nodes (122.8, 110, 100, 90, 72.5, 55, 45, 32.5, 20, 15, 10 and 0 km). The number of nodes is the minimum to provide a reasonable representation of a temperature profile. Temperature and temperature gradient were matched with the Bates profile at 122.8 km. Starting the cubic spline slightly above 120 km provided a better overall fit to the data. Densities below 122.8 km are calculated by first integrating up from 120 to 122.8 km with Bates temperature profile and, then, integrating down with the cubic spline profile. The harmonic expansion formulation has the intent of emphasizing terms of more importance to the lower atmosphere.

Unlike the thermosphere, in the lower atmosphere the diurnal variations aren't important as the annual variations. For this reason, daily temperature variations have been included only down to 72.5 km and were determined with the constraint that daily pressure variations be minimized below 50 km where variations are expected to be a few percent or less. This constraint may result in underestimating the daily temperature and pressure amplitudes in the mesosphere, but also data, obtained from existing rockets, aren't so accurate due to the difficulty to achieve these variations that are quite small relative to other ones. The $F_{10.7}$ and A_p variations have not

been carried below 110 and 90 km, respectively, where their coefficients became negligible and the pressure variations have to be minimized in the lower atmosphere. Unlike the MSIS-86 model, a latitude dependent acceleration of gravity has been used and this introduces a few percent change in density in the upper atmosphere at low and high latitudes. The main data constraint for this model below the 72.5 km was the MAP Handbook tabulations of zonal average temperature and pressure, as it was said above. For longitude variations, the tabulations of wave 1 amplitudes and phases were supplemented below 20 km by harmonic analysis of 9-year average of National Meteorological Center (NMC) data. The determination of the harmonic coefficients for the various nodes of the temperature profile is accomplished by a least squares fit to selected subsets of the data and subject to the constraints seen above.

Considering the average departures and standard deviations of the model from the input data in the lower atmosphere, the maximum departures from hydrostatic equilibrium are on the order of 5%. This isn't the error of density profiles because part of it results from the temperature and composition profiles. However, this level of error is similar to the overall average accuracy of upper atmosphere densities.

Over the 0 to 80 km altitude range, the zonal average monthly tabulations from the MAP Handbook differ from the MSISE-90 model by 1 K in temperature with a standard deviation of 3 K and by 1% in pressure with a standard deviation of 2%, although differences tend to be greater at the higher altitudes and latitudes. Near the 80 km, the MAP Handbook temperatures, densities and pressures are higher than the model by a few percent because this altitude region is where compromise in necessary to combine the model of upper atmosphere with the one of the lower atmosphere and where differences arise among data sources. Above 90 km the discrepancies between data and model increase due to the difficulty of making measurements and of modelling the greater range of natural variability and the importance of short-term variations (gravity wave and tidal). However, the standard deviations of densities from the model tend to be in the 15% and 20% range which is also typical for the upper atmosphere. Densities from the incoherent scatter technique, which provide the bulk of the data in the lower thermosphere, increase systematically with respect to the model for increasing altitudes.

The second harmonic in day of year isn't able to perfectly fit with the monthly changes in the MAP Handbook tabulations. Indeed, comparing the model with MAP Handbook points there are discrepancies in some months. However, considering the existing rockets data, there is no certainty that the month to month changes in the long-term average are enough known to justify a higher harmonic model for the long-term average. Year to year differences in the occurrence rate and severity of winter stratospheric warming events probably produce different month to month variations for various data samples.

The diurnal average mesopause minimum obtained by the MSISE-90 model is lower than the MSIS-86 one but is above the value found by von Zahn and Meyer. There are several modelling difficulties in reaching a minimum as low as that of von Zahn and Meyer. One is the geometrical difficulty of leaving a deep minimum with a strong positive temperature gradient and yet matching the given temperature and temperature gradient near the 120 km. The result is a temperature inflection at high summer latitudes between 90 and 120 km which is not consistent with the limited European Incoherent Scatter (EISCAT) data available. It may be possible some adjustment in the 120-km temperature and gradient at high summer latitudes which could help relieve this problem. Greater altitude resolution is also needed in the model near the mesopause to fit the von Zahn profile, but the available data indicate some variability in the height and the coverage is broader and not as a deep as the von Zahn profile. Tides have a role in determining the precise altitude and depth of the minimum, so that measurements need to be analyzed more systematically for local time effects. The matching of densities above and below the mesopause requires that a lower mesopause temperature be compensated by higher temperatures on either side, lower densities at the 120-km boundary or a change in composition.

The largest annual amplitude in temperature, density and pressure between the ground and the lower exosphere takes place in the upper mesosphere. The annual maximum is in summer except for a limited region near the mesopause and in the exosphere for density and pressure, because of helium and hydrogen bulge due to wind-induced diffusion, where the maximum is during the winter. The MSISE-90 model presents a notable semiannual temperature variation consistent with EISCAT temperatures, unlike the MSIS-86 one. For example, at mid latitudes and 105 km height the peak amplitude is 8 K compared to the 11 K for incoherent scatter data and the 1 K for MSIS-86. Contrariwise, there isn't a significative semiannual density variation that would be expected to result from the temperature one.

Diurnal and semidiurnal variations cause peak amplitudes in the lower thermosphere, due to tides in the lower atmosphere, and increase in the upper thermosphere, due to in situ heating. Daily temperature variations fit quite well to the measurements obtained by incoherent scatter data and rockets at low and mid latitudes near the lower thermosphere peak. The data above 100 km are mainly incoherent scatter which is limited to daytime conditions, specially at low altitudes. MSISE-90 model is slightly better in this region than previous one but makes a more realistic transition into the mesosphere. Regarding model semidiurnal density amplitudes in the lower thermosphere, they don't represent realistically data as temperature variations did.

Considering the longitude variations, there is a maximum at high winter latitudes as expected from the MAP Handbook. Wave amplitudes show a regular phase change with altitude in lower atmosphere, are almost null in the lower thermosphere, where there is a lack of longitude

coverage data to define a longitude variation in temperature or density, and increase above 150 km where satellite data show temperature and density maxima around magnetic poles.

1.2.4. NRLMSISE-00

The NRLMSISE-00 model, developed in 2000 by Mike Picone, Alan Hedin and Doug Drob, is an upgrade of MSISE-90 in the thermosphere [6]. The new model includes all data of the previous MSIS-class models but adds also both drag measurements, on which Jacchia models were based, and satellite accelerometer data. Thanks to drag and accelerometer data on total mass density, the NRLMSIS database should improve the statistical predictions of density over the previous models and this could influence the model coefficients for temperature and composition. The Millstone Hill data on lower thermospheric temperature (T_{low}), at a height between 100 and 130 km, allow to check and reinforce MSIS temperature model parameter and better define the model near the mesopause, because the neutral temperature is approximately equal to the ion temperature, so that extraction of information is simple.

New important data are ones of Solar Maximum Mission (SMM) which provide molecular oxygen number density [O_2] over the altitude between 140 and 220 km and over a wide range of solar activity. Indeed, before this mission there weren't direct measurements of O_2 above 150 km at high solar activity. The SMM occultation measurements suggest that dissociation may increase sufficiently to keep density constant at 200 km as solar activity increases. These data allow to determine dependence on the solar EUV and on the magnetic activity. At this point, there was a contrast between mass spectrometer data and MSISE-90 profiles of $O_2(z)$, that consider oxygen molecules in approximate diffusive equilibrium above 150 km, and occultation observation of $O_2(z)$, that fall below diffusive equilibrium values by an increasing amount. To smooth these differences, the NRLMSISE-00 model modified the parametrization of the lower thermospheric altitude profiles of O_2 and O. So, the model is a statistical compromise between the two data sources in the altitude region covered by SMM data.

Another important addition to the NRLMSIS model is an "anomalous oxygen" component to high-altitude drag and total mass density at the summer high latitudes. Above 500 km, this component increases the thermospheric total mass density attributable to the neutral species in diffusive equilibrium at the thermospheric temperature. The anomalous oxygen component causes the presence of hot atomic oxygen (O_h) or atomic oxygen ions (O^+) near the exobase under some conditions but it isn't possible distinguish exactly contributions by the two species and, therefore, their individual effects. Analysis of data and empirical models, in 1989, led Hedin to infer an additional non-thermospheric oxygen component to the total mass density near the exobase. In particular, he found that an appreciable hot atomic oxygen (O_h) population could be present at high latitude and high altitude, above 600 km, in the summer hemisphere.

Indeed, under the additive condition of high solar activity, he observed that the atomic oxygen population of MSIS-86 model was lower than measurements of the neutral mass spectrometer aboard of Dynamics Explorer 2 (DE 2). Under the same conditions, but with low to moderate solar activity, the Jacchia-70 model showed significant higher total mass density compared to MSIS-86 and, therefore, Hedin supposed that, given the according result of the DE 2 analysis for high solar activity, the Jacchia-70 raising could be caused by an appreciable hot atomic oxygen geocorona under those conditions. Towards the end of 90's, analyses of Incoherent Scatter Radar (ISR) data have demonstrate that a small, but not negligible, O_h component can account for a theoretical deficit in ion heating in the upper thermosphere. During the same period, Keating et al. analyzed neutral and ion mass spectrometer instruments aboard the Midcourse Space Experiment (MSX) [7]. MSX flew in a Sun-synchronous (near-polar) circular orbit at 900 km during a solar minimum. Keating et al. observed discrepancies in the respective Jacchia-70 and MSIS estimates of He and total mass density as MSX transited the summer pole. The MSX neutral composition data showed that the increase of total mass density, under these conditions, is due to O^+ and not to higher values of He. Another important discovery was that the mass density of O^+ is higher than the other ionic species (H^+, He^+, etc.). The data used to estimate anomalous oxygen were the drag data sets of Jacchia and Barlier (JB) above 600 km that measured both O_h atoms and O^+ ions, while the DE 2 neutral mass spectrometer data weren't used because they measure only neutral species. Moreover, DE 2 data have limit due to the lack of points above 600 km that cover only high solar flux and a narrow temporal range. However, a comparison between JB and DE 2 data showed a good qualitative agreement at high latitudes and elevated solar flux.

Last additive data for this new model are the Millstone Hill and Arecibo incoherent scatter ones on exospheric temperature (T_{ex}), from 1981 to 1997. These data result from fitting a model of ion heat balance and chemistry to the ion temperature profile using ISR observables and parameterized models of neutral oxygen and temperature. The extraction of T_{ex} from the ISR data didn't include a hot oxygen component. The new data, when compared with the previous MSIS ones, have changed their solar activity dependence both for the temperature and the mean total mass density, especially at high altitudes. Indeed, at the exosphere, the NRLMSISE-00 T_{ex} is above that of MSISE-90, about few degrees, at low latitudes and for moderate to low $F_{10.7}$, while, when solar flux increases, the T_{ex} value for NRLMSISE-00 falls below that of MSISE-90 by a steadily increasing amount.

1.2.5. Models comparison

The choice of the model to use for the orbit determination and propagation of satellites and, so, the estimate of their decay isn't always the same. It depends on several factors: the altitude of

the orbit, the satellite parameters, as mass, drag coefficient and area, the solar and magnetic activity and the necessary accuracy of computation. Indeed, isn't true that last model is the more accurate in all operative conditions.

An example is the study done by Anselmo et al. [3][8], which did a comparison between Jacchia-71 and MSISE-86/90, by analyzing the orbital decay of nine spherical satellites in the 150-1500 km altitude range. The study was led during a complete solar cycle, but not all satellites were operating during this period. The comparison is done between the theoretical drag coefficient, obtained by the drag equation

$$\vec{D} = -\frac{1}{2} C_D \frac{A}{M} \rho \vec{V}_R \left|\vec{V}_R\right| \tag{1-6}$$

where $\vec{D}$ is the drag acceleration, C_D is the drag coefficient, A is the cross-sectional area perpendicular to the direction of the air flow, M is the satellite mass, $\vec{V}_R$ is the relative velocity of the satellite with respect to the atmosphere and ρ is the atmospheric density obtained by the considered model, and the measured C_D. Therefore, all the results obtained, presented in table 1.2, must consider the additive uncertainty of the drag coefficient of 15%. At 1500 km both models underestimate more than 60% the air density at low solar activity conditions, while at high solar activity they have better performances and J-71 is even better than MSISE-86/90. Below 800 km the performances of all models are much better than at previous altitudes, especially, at moderate solar activity. At 750-800 km, during low solar activity conditions, both two models underestimate the air density, although discrepancies are comparable with to the drag coefficients uncertainties. The major differences are at high solar activity where J-71 is almost 10% better than MSISE-86/90. Below 400 km, the results are similar except for moderate solar activity at 350-390 km altitude range where J-71 is again better than MSIS-86/90.

Altitude (km)	Solar activity conditions		
	Low	Moderate	High
1500	MSIS-86/90: +62% J-71: +62%		MSIS-86/90: +34% J-71: +10%
750-800	MSIS-86/90: +7%/+17% J-71: 0/+9%	MSIS-86/90: +6% J-71: +6%	MSIS-86/90: +16% J-71: -2%
350-390	MSIS-86/90: 0 J-71: -4%	MSIS-86/90: +15% J-71: +2%	
150-350	MSIS-86/90: -11%/-19% J-71: -20%/-25%	MSIS-86/90: +5% J-71: +3%	

Table 1.2: differences between estimated and theoretical drag coefficients [8]

Another kind of comparison could be done to vary the geomagnetic index among all the models described below [6]. To compare the models shown above, two factors will be used: the weighted mean (β) of the residuals and the corresponding standard deviation (σ)

$$\beta = \langle d_i - m_i \rangle \tag{1-7}$$

$$\sigma = [\langle (d_i - m_i)^2 \rangle - \beta^2]^{1/2} \tag{1-8}$$

where d_i is a data set and m_i is the corresponding model estimates. Therefore, the mean residual indicates the magnitude of systematic differences between a data set and corresponding model estimates. If β is positive the model underestimates the measured values on average, otherwise, negative β means overestimation of the model. The standard deviation, instead, measures the agreement between the geophysical variability contained in the model and the geophysical variability implicit in measurements of database.

A_p	Altitude (km)	Points	N00		M90		J70	
			Mean	SD	Mean	SD	Mean	SD
≤ 10	200-400	6236	-0.06	0.17	-0.06	0.17	-0.04	0.17
	400-800	10041	-0.07	0.23	-0.08	0.26	-0.07	0.25
	800-1200	5586	0.01	0.23	0.03	0.27	-0.05	0.23
	>1200	15	0.20	0.09	0.27	0.10	-0.18	0.05
All	200-400	10456	-0.07	0.17	-0.06	0.17	-0.07	0.19
	400-800	16021	-0.08	0.25	-0.07	0.27	-0.09	0.28
	800-1200	9373	0.01	0.24	0.04	0.27	-0.07	0.25
	>1200	24	0.22	0.12	0.30	0.11	-0.20	0.13
≥ 50	200-400	304	-0.05	0.23	-0.07	0.23	-0.12	0.25
	400-800	441	-0.01	0.36	0.01	0.39	-0.17	0.42
	800-1200	282	0.07	0.35	0.05	0.39	-0.14	0.39

Table 1.3: statistical comparison of empirical models to Jacchia data [6]

Table 1.3 shows the mean residual and the standard deviation of all the models at different geomagnetic activities. At low to moderate geomagnetic activity the results of the three models are almost comparable. At high geomagnetic activity, instead, the standard deviation of both MSISE-90 and J-70 models are higher than that of NRLMSISE-00. Moreover, the mean residual of J-70 model, under these conditions, is considerably larger than the residuals of MSIS models, meaning that it overestimated the data. A last feature, shown by this comparison, is that all the mean residual of J-70 are negative, overestimating data at all altitudes, while MSIS models have a positive mean residual at high altitudes and a negative one at lower altitudes. This difference is linked with the nonoptimal match of J-70 with the $F_{10.7}$ variability of data.

Chapter 2

Satellites with on-board accelerometer: GRACE's case

To evaluate more directly the atmospheric density, it's necessary that satellites measure accelerations on-board. This chapter describes Gravity Recovery and Climate Experiment (GRACE) mission, which carry on-board SuperSTAR accelerometers. After a brief description of GRACE satellites, we focus on data that will be used to calculate atmospheric drag.

2.1. History

The first satellites that carried precise accelerometers were Challenging Minisatellite Payload (CHAMP), launched in 2000, and the twins Gravity Recovery and Climate Experiment (GRACE), launched in 2002. Afterwards, other satellites, as Gravity Field and Steady-State Ocean Circulation Explorer (GOCE) in 2009, or SWARM ones, in 2013, were launched, but none of them had as main objective the study of the thermosphere (density and winds). They carried accelerometers in order to remove nongravitational signals from measured orbit perturbations due to inhomogeneities in the Earth's gravity field. However, their application to thermosphere studies has resulted in density and wind data sets containing information at unprecedented levels of detail and coverage.

The increased use of the accelerometers is due partly to a rise in the instrument's sensitivity that, at the beginning of this century, has increased by several orders of magnitude, making them suitable for use at higher altitudes in which there is less drag force.

2.2 Mission

Gravity Recovery and Climate Experiment (GRACE) was born from the partnership of NASA and the German Center for Air and Space Flight. It was a scientific mission that had to track how water is transported and stored within the Earth's environment. In particular, it measured anomalies of the planet gravity field that allowed to estimate the variations of water masses, yielding new information on effects of global climate change.

The twin GRACE satellites were launched in March 2002 from Russia on a five-year mission [9]. Actually, they ended their work about ten years later: in October 2017, GRACE-B, and in March 2018, GRACE-A, because of the exhaustion of batteries. They have flown a polar orbit (89 deg inclination) 500 km over the Earth and separated by 220 km along the track. The altitudes decayed in tandem during the lifetime mission from the 500 km at the beginning to 300 km and lower at the end.

GRACE's main objectives were:

- obtain very high-resolution global models of Earth's gravity field, including how it varies over time. These estimates provided a complete understanding of how mass is distributed globally and how that distribution varies over time.
- improve the study of the Earth's ionosphere through the use of a particular technique called "GPS limb sounding" that allows to quantify total electron and/or refractivity in the ionosphere and troposphere, measuring the delay of GPS signals that pass through Earth's ionosphere and atmosphere.

Figure 2.1: GRACE twin satellites in orbit around the Earth. Credit: NASA

2.2. Spacecraft

The two GRACE satellites are identical except for transmit and receive frequencies. Each satellite measures 1,94 meters in width, 3,12 meters long and 0,72 meters high and has an initial mass of 487 kg [9]. They flied facing each other, one forward and one backward, so they could

point the microwave k-band antennas at each other. The outer shell of each satellite was covered by silicon solar cell arrays (figure 2.1) that provided the electrical energy to the instruments and satellite bus users. The excess energy is stored in a battery of 10 nickel-hydrogen cells that provide up to 16 amp-hours of 28-volt power per satellite.

The microwave K-band ranging instrument was the most important for GRACE because it provided precise measurements (within 1 micron) of distance between the two satellites. It was made up of an ultra-stable oscillator, that needed as the frequency and clock reference for satellite, a K-band ranging horn, to transmit and receive K-band (24 GHz) Ka-Band(32GHz) signals to and from the other GRACE satellite, a sampler, that downconverted and sampled the incoming signal phases, and instruments processing unit, to provide digital signal processing functions for the K and Ka band signals, but also for GPS. Each satellite, indeed, carried on board a GPS receiver, called "Black Jack", to determine the exact position of the satellites in orbit and provide the possibility to conduct atmospheric occultation experiments. The system uses three antennas; one to collect navigation data, while the other two were used to store backup navigation and atmospheric occultation data collection.

Each satellite mounted two star cameras, with a field of view of 18 deg by 16 deg, both for science purposes and attitude and orbit control; laser retro-reflectors on the underside, for backup and orbit verification purposes; an on-board data handling system, which acted as the central processor and it was able to manage the science and housekeeping data, provide input and output to other subsystem as attitude and control one or thermal one and carry out operations for the health of satellite, including fault detection, isolation of components and recovery operations.

The telemetry and telecommand subsystem was formed by an S-band boom antenna, that deployed after launch by a pyrotechnic device and communicated with Earth via radio systems in the microwave S-band spectrum (2-4 GHz). There were other backup antennas on the top and the bottom of the satellite to provide backup communication in case of failure of the main system.

The satellite was "three-axis stabilized" and the attitude and orbit control were monitored by a series of sensors, actuators and software. The main sensor was the star camera assembly and, in addition to this, there were three other elements: an Earth-Sun sensor, that provided an attitude determination during all the phases of the mission; a gyro, that provided attitude rates during the emergency situations; a magnetometer, that provided coarse attitude based on the satellite position obtained by on-board GPS position and a model of Earth's magnetic field. An inertial reference unit provided three-axis rate information. A Forster magnetometer was mounted on the deployable boom to provide additional rate information. A reaction control system and six magnetorquers were present on-board as attitude controllers. The first one used

gaseous nitrogen stored in the two tanks along the main satellite axis, the other one, used for fine corrections of orientation, helped to minimize the satellite consumption over the mission lifetime. Two orbit-control thrusters, each of which provided 40 millinewton of thrust, were mounted on the rear-panel of each satellite to adjust its orbit.

The thermal control was done using a combination of active and passive control elements. It consisted of 64 independent thermistor-controlled heater circuits for monitoring in-flight temperature and heater and for on-ground verification testing. Each satellite carried on-board an accelerometer to measure the non-gravitational forces acting on it. There was, also, a mass trim system to maintain the spacecraft center of gravity aligned to the center of the proof-mass of accelerometer.

Of course, most systems on the satellites were fully redundant to avoid the loss of spacecraft's elements in case of device failures. All the spacecraft subsystems, instruments, fuel tanks and batteries were mounted on a carbon-fiber reinforced plastic platform. This material has a very low coefficient of thermal expansion and, so, it allows the precise measurements between the two satellites.

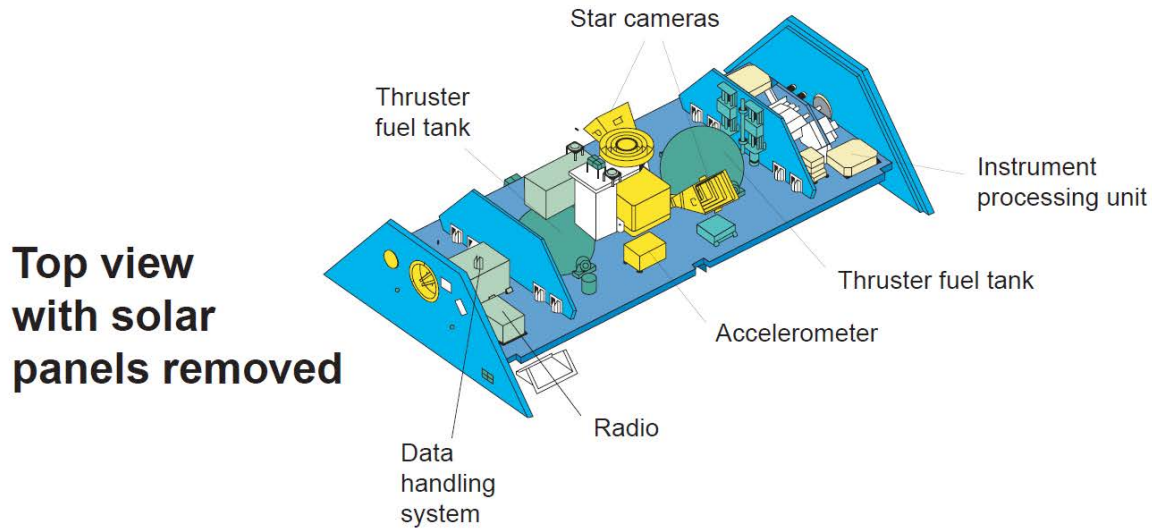

Figure 2.2: top view of GRACE spacecraft with solar panels removed. Credit: ESA

2.3. Accelerometers

Each GRACE satellite carried on-board a Super Space Three-axis Accelerometer for Research mission (SuperSTAR): an accelerometer developed by ONERA/CNES, which had the precise goal of measuring of all non-gravitational accelerations (drag, solar and Earth radiation pressure) acting on the GRACE spacecraft. The measurement principle of SuperSTAR is based on the electrostatic suspension of a parallelepipedic proof mass inside a cage. The cage walls have control electrodes that serve both as sensors to measure the instantaneous proof mass (PM) position and as actuators to apply electrostatic forces to maintain the PM in the center of the cage.

Figure 2.3: sensor unit (right) and the ICU (left) of the SuperSTAR accelerometer. Credit: ONERA

The configuration of the two SuperSTAR accelerometers takes advantage of the CHAMP mission experience. The improvement of the performances with respect to STAR comes mainly from the increased gap between the proof-mass and the sensitive axes electrodes: 175 μm instead of 75 μm in the CHAMP model and also of the modification of electronics function parameters as, for example, the reduction of the bias reference voltage by a factor 2, a better adjustment of the measurement conditioning amplifiers and an optimized exploitation of the 24 bit sigma-delta analog to digital converters.

SuperSTAR was mounted at the center of gravity of the satellite and consisted of the following elements: Sensor Unit (SU), Electromagnetic Exciting Unit (EEU), Interface Control Unit (ICU), and a harness. SU was a metallic proof mass, suspended inside an electrode cage of gold-coated silica. The proof mass motion was servo-controlled using capacitive sensors. The mass and electrode cage core were enclosed by a sole plate and a housing in which vacuum was maintained using a getter. The SU vacuum unit was surrounded by analog electronics. The EEU was used to deliver a 10 mg acceleration and was used only in case of an SU start-up

problem. The ICU supplied power to the SU and EEU and operated the accelerometer through a micro-controller board.

2.4. Data

As it was said above, there are satellites more recent than GRACE ones, but, for this thesis, it was decided to use GRACE due to the availability of its data, that are archived and distributed through two agencies:

- *JPL Physical Oceanography Distributed Active Archive Center (PO.DAAC)*
  The PO.DAAC is one element of the Earth Observing System Data and Information system (EOSDIS), developed by NASA. The goal of the PO.DAAC is to serve the needs of the oceanographic, geophysical and interdisciplinary science communities that require physical information about the oceans.

- *GeoForschungsZentrum Potsdam (GFZ)*
  The GFZ is a non-university geoscientific research institute that combines all solid Earth science fields including geodesy, geology, geophysics, mineralogy and geochemistry, in a multidisciplinary research center.

GRACE data had different processing [10] [11]. The first data, called *Level 0 Data*, are the result of the telemetry data reception, collection and decommutation by the GRACE Raw Data Center (RDC) at DLR in Neustrelitz. Data for each pass, from each satellite, are separated into the science instruments and spacecraft housekeeping data streams and placed in a rolling archive at the RDC. Afterwards, GRACE Science Data System (SDS) acquires data and separates into respective instrument packets with a non-destructive processing: data are converted from binary encoded measurements into engineering units thanks to a sensor calibration factors. Editing and quality control flags are added, and, where necessary, the time tags are corrected to the respective satellite receiver clock time. This level, denoted as *Level 1A Data*, includes the ancillary data products needed for processing to the next level. A possibly irreversible processing is, then, applied to both *Level 0 Data* and *Level 1A Data* and provides *Level 1B Data*. Data are correctly time-tagged and the samples rate is reduced from the high rate samples of previous levels for further science analysis. This level also includes the ancillary data products generated during this processing, and the additional data needed for further processing. The last process allowed to obtain the *Level 2 Data*: instruments measurements over several days are consolidated into a sequence of gravity field estimates, representing the time-variable and average Earth gravity field models.

All level 1B data are in binary format, but they can be converted in ASCII format by using *Bin2AsciiLevel1*, a software utility, in UNIX language, that can be downloaded with Level 1B data [26].

Different coordinate systems are used to define the various GRACE data products. Among all of these, the ones will be used during this work are:

- *Science Reference Frame (SRF)*: its origin is the target location of the accelerometer's proof mass and it has coordinate axes directed: X_{SRF}, from the origin to the K/Ka band horn, namely towards the other satellite (roll axis); Y_{SRF}, to complete a right-handed triad with the other two axes (pitch axis); Z_{SRF}, from the origin to the plane of the main equipment platform, positive towards the satellite radiator and normal to X_{SRF} (yaw axis).
- *Accelerator Frame (AF)*: its origin is the center of mass of the proof mass of the accelerator and it has coordinate axes parallels to the SRF and directed in the following way: X_{ACC} // Y_{SRF}, Y_{ACC} // Z_{SRF}, Z_{ACC} // X_{SRF}.
- *Terrestrial Frame (TF)*: its origin is the center of mass of the Earth and the three axes are: X_{TF}, defined as is the intersection between the equatorial plane and the mean Greenwich meridian, Y_{TF}, orthogonal to the other two axes so the system is right-handed, Z_{TF}, directed towards the Conventional Terrestrial Pole (CTP),

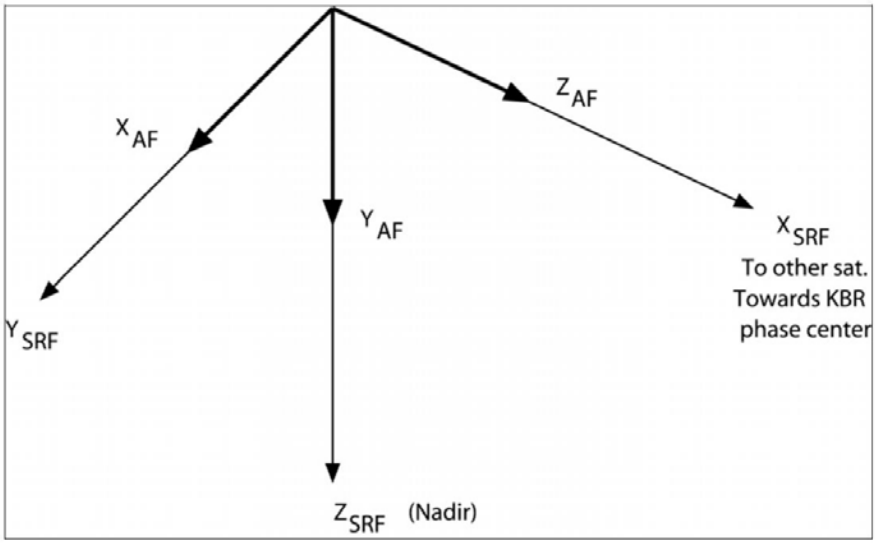

Figure 2.4: Satellite body-fixed frames [10]

During flight, the satellites have nadir-pointing yaw-axis orientation, with the roll axes in the anti-flight and in-flight directions for the leading and trailing satellites, respectively.

2.4.1. Accelerometer data

The accelerometer data provide the linear and angular acceleration components of the proof mass of each satellite for each second. Level 1A Data are pre-processed and quality flags are checked. Data gaps of 10 seconds or shorter are filled with a quadratic interpolation when at least two points per side are available, otherwise, a linear interpolation is used to fill gaps. Data gaps of more than 10 seconds aren't filled.

The accelerations that we find in the accelerometer level 1B data (ACC1B) have an instrument scale and bias offset [12]. Therefore, the bias and scale corrections must be applied to data for each axis of the two satellites in the following way:

$$f_{new} = bias + scale * f_{acc1B} \tag{2-1}$$

The value of scale factor is

Direction (SRF)	GRACE-A	GRACE-B	Uncertainty
X	0.9595	0.9465	±0.002
Y	0.9797	0.9842	±0.02
Z	0.9485	0.9303	±0.02

The bias, instead, varies over time, so it can be modeled by a quadratic over a large duration. The general form for the bias is:

$$bias = c_0 + c_1(T_d - T_0) + c_2(T_d - T_0)^2 \tag{2-2}$$

where T_d is the modified Julian date ($T_d = JD - 2{,}400{,}000.5$).

Coefficients and T_0 are estimated through different periods of the mission (all elements in the tables have units of μ/s^2):

- Data before the 7th March 2003: $T_0 = 52532$

Direction	C0	C1	C2	Residual
Grace-A Xsrf	-1.106	2.233E-4	2.5E-7	0.003
Grace-A Ysrf	27.042	4.46E-3	1.1E-6	0.053
Grace-A Zsrf	-0.5486	-1.139E-6	1.7E-7	0.019
Grace-B Xsrf	-0.5647	-7.788E-5	2.4E-7	0.002
Grace-B Ysrf	7.5101	7.495E-3	-9.6E-6	0.080
Grace-B Zsrf	-0.8602	1.399E-4	2.5E-7	0.020

- Data after the 7th March 2003: $T_0 = 53736$

Direction	C0	C1	C2	Residual
Grace-A Xsrf	-1.2095	-4.128E-5	9.7E-9	0.002
Grace-A Ysrf	29.3370	6.515E-4	-3.9E-7	0.056
Grace-A Zsrf	-0.5606	-2.352E-6	3.8E-9	0.020
Grace-B Xsrf	-0.6049	-1.982E-5	3.5E-9	0.002
Grace-B Ysrf	10.6860	1.159E-3	-4.3E-7	0.076
Grace-B Zsrf	-0.7901	4.783E-5	-6.5E-9	0.020

ACC1B data are referred to Science Reference Frame.

2.4.2.GPS Navigation Data

GPS navigation level 1B data (GNV1B) provide precise GRACE satellite orbit ephemerides every 5 seconds. These data give information about position, velocity and their relative errors. All GNV1B data are referred to Terrestrial Frame.

2.5. Geometry and properties

Each GRACE spacecraft can be split into a macromodel of 8 flat plates, but for the purpose of this thesis the deployable boom is negligible because its area is 10^{-2} m^2 smaller than other surfaces, so 6 flat plates will be considered. As shown in table 2.1, the surface properties will be introduced. For each plate are provided area, the components of its unit normal in the Science Reference Frame, the material and its emissivity and absorptivity/reflectivity coefficients. Each surface has four reflectivity coefficients because reflect both in visible and in infrared range and, not being completely smooth, has a reflection both specular and diffusive. This last coefficient, in particular, is quite difficult to estimate because it requires a complex three-dimensional model of the satellite.

During GRACE mission, the spacecraft varied its mass from the 487.2 kg at launch. To take into account the loss, mass was modeled for GRACE-A and GRACE-B respectively, as:

$$m_A = 482.6 - 0.0061 * (TMJD - 52{,}850) \tag{2-3}$$

$$m_B = 482.69 - 0.0038 * (TMJD - 52{,}850) \tag{2-4}$$

where TMJD is time in modified Julian date format [13].

Panel	Area (m^2)	Unit Normal			Material	Emiss (IR)	Absorp (Vis)	Refl (Vis)		Refl (IR)	
		X	Y	Z				Specular	Diffusive	Specular	Diffusive
Front	0.95551567	+1.0	0.0	0.0	SiOx/Kapton	0.62	0.34	0.40	0.26	0.23	0.15
Rear	0.95551567	-1.0	0.0	0.0	SiOx/Kapton	0.62	0.34	0.40	0.26	0.23	0.15
Starboard	3.1554792	0.0	+0.76604	-0.642787	Si Glass Solar Array	0.81	0.65	0.05	0.30	0.03	0.16
Port	3.1554792	0.0	-0.76604	+0.642787	Si Glass Solar Array	0.81	0.65	0.05	0.30	0.03	0.16
Nadir	6.071112	0.0	0.0	+1.0	Teflon	0.75	0.12	0.68	0.20	0.19	0.06
Zenith	2.167362	0.0	0.0	-1.0	Si Glass Solar Array	0.81	0.65	0.05	0.30	0.03	0.16

Table 2.1: geometry and properties of each surface of GRACE spacecraft [11]

Chapter 3

Density Retrieval Procedure

SuperSTAR accelerometers on-board of GRACE spacecrafts measure the sum of all forces on the satellite's surface. At the GRACE heights, the predominant force is the atmospheric drag, but also solar and Earth radiation pressure are not negligible. By modeling the effects of these last forces, we obtain a method of isolating the acceleration caused by drag. The modeled accelerations can be subtracted from the total nongravitational forces, measured by the accelerometers.

Because GRACE lifetime mission covers more than one entire solar cycle, it was possible to investigate the variations between model and real data at all solar activity, as shown in figure 1.1. Three periods of time were considered: 1st of August to the 27th of August 2002, where the solar activity has its maximum, 1st of June to the 30th of June 2008, at moderate solar activity, and 1st of June to the 30th of June 2012, where solar activity has its minimum. For each interval of time, data were taken every 10 minutes to have a wide temporal coverage, about 9 points per orbit, without have a computational requirement too severe; moreover, this choice allows to have satellite into different positions over the Earth. Another important factor is the value of the surface properties; for the purpose of this thesis the nominal values are used even if this should bring further uncertainty, especially when several years are passed from the beginning of the mission. So, the numbers of tab 2.1 was used without correction coefficients. Finally, because the two satellites are basically identical, all the study is done for GRACE-A and, as we said in the previous chapter, the macromodel is formed by 6 flat plates.

3.1. Acceleration data

First of all, accelerations of GRACE-A spacecraft were extracted from the *"GRACE LEVEL 1B JPL RELEASE 2.0"* provided by PO.DAAC [26]. As it was seen above, data have to be corrected from bias and scale factor, according to equation 2-2. Because data for moderate and low solar flux are several years later than 2003, it was necessary make some corrections about coefficients of equation.

3.2. Solar-radiation pressure

Solar radiation pressure (SRP) is an important perturbative force due to photons emitted by the Sun, that, when hit the satellite surface, transfer their momentum. The average flux of momentum is quite constant during the year, varying about ±3% due to variations of distance between Earth and Sun. However, the SRP becomes more influential at higher altitudes. Indeed, below 400 km the drag forces are notably larger than other perturbations, while between 400 and 600 km, where were GRACE satellites, the differences between drag forces and solar radiation pressure start to be smaller. Above 600 km, SRP becomes predominant relative to the drag force, which decreases until zero above 1000 km.

The acceleration due to solar radiation can be compute by the following equation [23][24]:

$$\vec{a}_{SR} = \sum_{i=1}^{6} -\frac{RA_i \cos(\Phi_{inc,i})}{mc}\left\{2\left(\frac{C_{rd,i}}{3} + C_{rs,i}\cos(\Phi_{inc,i})\right)\hat{n}_i + (1 - C_{rs,i})\hat{s}\right\} \qquad (3\text{-}1)$$

where R is the incoming solar radiation flux [27][28], A_i is the area of plate hit by the Sun, $\Phi_{inc,i}$ is the angle of incidence of the Sun with respect the plate, m is the satellite's mass (see eq. 2-3), c is the speed of light, $C_{rd,i}$and $C_{rs,i}$ are the coefficient of diffusive and specular reflectivity respectively, $\hat{n}_i$ is the unit plate normal and $\hat{s}$ is the unite satellite-Sun vector.

The magnitude of solar flux is multiplied by a ratio to account for how much incoming solar radiation hits the satellite. Finding the Sun-Earth vector and the appropriate flux acting on the satellite required an up-to-date Jet Propulsion Laboratory solar and planetary ephemerides (version DE-405) [30].

Solar ephemerides are in the Terrestrial Frame, so a matrix rotation is used to translate vectors from TF to SRF:

$$M_{TF}^{SRF} = \left(\begin{bmatrix}\cos(-\Omega) & \sin(-\Omega) & 0\\ -\sin(-\Omega) & \cos(-\Omega) & 0\\ 0 & 0 & 1\end{bmatrix}\cdot\begin{bmatrix}1 & 0 & 0\\ 0 & \cos(-i) & \sin(-i)\\ 0 & -\sin(-i) & \cos(-i)\end{bmatrix}\cdot\begin{bmatrix}\cos(-u) & \sin(-u) & 0\\ -\sin(-u) & \cos(-u) & 0\\ 0 & 0 & 1\end{bmatrix}\right)^{T} \qquad (3\text{-}2)$$

where u is the argument of latitude, i is the inclination and Ω is the longitude of the ascending node.

3.3. Albedo and infrared radiation pressures

Albedo and infrared pressures are other two perturbative forces, smaller than the previous ones, but not negligible. The formula to calculate the effect of each Earth element on each satellite plate is [14]:

$$\vec{a}_{EA} = \sum_{i=1}^{6} \sum_{j} -\frac{R_j A_i \cos(\Phi_{inc,ij})}{mc} \left\{ 2\left(\frac{C_{rd,i}}{3} + C_{rs,i}\cos(\Phi_{inc,ij})\right)\hat{n}_i + (1 - C_{rs,i})\hat{s}_j \right\} \quad (3\text{-}3)$$

where R_j is the flux originating from the source j [30], A_i is the plate area, $\Phi_{inc,ij}$ is the angle of incidence of the source with respect the plate, m is the satellite's mass (see eq. 2-3), c is the speed of light, $C_{rd,i}$and $C_{rs,i}$ are the coefficient of diffusive and specular reflectivity respectively, $\hat{n}_i$ is the unite plate normal and $\hat{s}_j$ is the unite satellite-source vector.

For the purpose of this thesis, $\hat{s}_j$ is always the unite satellite-Earth vector given by GNV1B data at that moment. Therefore, to consider the field of view of the satellite the albedo radiation is:

$$R_{j,alb} = R * a * \sin^2(2\eta_{horizon}) \quad (3\text{-}4)$$

while the infrared radiation is:

$$R_{j,ir} = IR * \sin^2(2\eta_{horizon}) \quad (3\text{-}5)$$

where a is the percentage of albedo effect, the planetary Earth albedo (ie., averaged over the entire Earth) varies from 0.25 to 0.35, IR is the infrared energy emanating at the Earth's surface and $\eta_{horizon}$ is the angular radius of the Earth seen from the satellite [23]:

$$\sin(\eta_{horizon}) = R_{earth}/r_{sat} \quad (3\text{-}6)$$

where R_{earth} is the Earth radius and r_{sat} is the distance from the satellite to the center of the Earth.

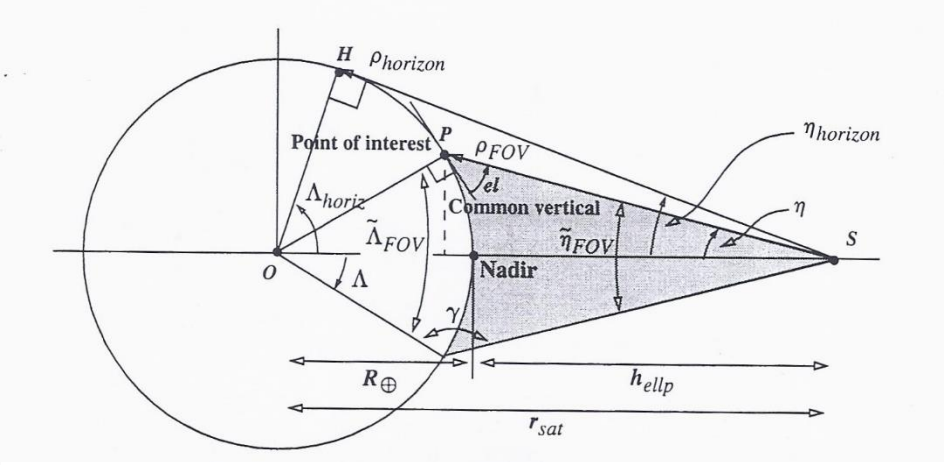

Figure 3.1: Basic Geometry for Field of View-Nadir Pointing [23]

For both albedo and infrared accelerations, the predominant component is along the z-axis, because this axis is directed towards the Earth, while the other two are on the perpendicular plane to it. Therefore, the principal panel which is hits by radiation is the one facing the Earth.

3.4. Atmospheric drag

Atmospheric forces are the largest non-gravitational disturbances acting on satellites in low orbit. However, precise modeling of them it's very difficult to three reasons. Firstly, the physical properties of the atmosphere, and in this case the main element it's the density of upper atmosphere, aren't know very accurately. Then, we would need a specific knowledge of the of the interaction of neutral gas and of charged particles with the different spacecraft surfaces. At last, we need to consider the varying attitude of non-spherical satellites with respect to the atmospheric particle flux.

The dominant atmospheric force acting on satellites, called drag, is directed opposite to the velocity of the satellite motion with respect to the atmospheric flux, hence decelerating the satellite. For this reason, drag is a nonconservative perturbation because friction causes a loss of energy and, so, the total energy isn't constant. Minor contributions to atmospheric forces are the lift force and binormal forces, acting perpendicular to this relative velocity, that can be neglected in the free-molecular-flow regime.

The basic equation for aerodynamic drag combines different factors. As we are interested in accelerations, the formula for drag is:

$$\vec{a}_{drag} = -\frac{C_D A}{2m}\,\rho {v_{rel}}^2 \frac{\vec{v}_{rel}}{|\vec{v}_{rel}|} \tag{3-7}$$

where C_D is the drag coefficient, A is the exposed cross-sectional area, the area normal to the satellite's velocity, ρ is the atmospheric density, m is the satellite's mass (see eq. 2-3) and $\vec{v}_{rel}$ is the velocity of the satellite with respect to the surrounding atmosphere. We can separate $\vec{v}_{rel}$ into two components [14]: the velocity of the satellite with respect to an atmosphere that corotates with the Earth, $\vec{v}_c$, and the velocity of any deviation in wind speed, $\vec{w}_c$. So $\vec{v}_{rel} = \vec{v}_c - \vec{w}_c$.

3.4.1. Drag coefficient

The coefficient of drag C_D is a dimensionless quantity that describes the interaction of the atmosphere with the satellite's surface materials. Values of C_D are certainly major then 2.0,

even if a priori knowledge of C_D is very difficult, because it depends on the spacecraft surface material, the chemical constituents of the atmosphere, the molecular weight and the temperature of the impinging particles [15] [16].

For this thesis, the drag coefficient is calculated by the Cook's formula [17][18]:

$$C_D = 2\left[1 + \frac{2}{3}\sqrt{1 + \alpha\left(\frac{T_w}{T_i} - 1\right)}\cos\theta\right] \tag{3-8}$$

where α is the energy accommodation coefficient, T_w is the wall temperature, T_i is the kinetic temperature of incident particles with mass velocity V and θ is the angle of incident gas flow with to respect the satellite surface. For a particle gas, the kinetic temperature is given by $(3/2)RT_i = (1/2)V_i^2$, where R is the mean gas constant of atmosphere. Consequently

$$T_i = \frac{1}{3R}V^2 \tag{3-9}$$

and

$$C_D = 2\left[1 + \frac{2}{3}\sqrt{1 + \alpha\left(\frac{T_w}{V^2/(3R)} - 1\right)}\cos\theta\right] \tag{3-10}$$

For practical application the wall temperature influence disappears in Cook's model:

$$C_D = 2\left[1 + \frac{2}{3}\sqrt{1 - \alpha}\cos\theta\right] \tag{3-11}$$

Formulas written are valid for inclined surface elements. The drag coefficient due to molecules incident on flow parallel surfaces is given by

$$C_{Dp} = \frac{1}{\pi}\frac{1}{S} \tag{3-12}$$

where S is the molecular speed ratio.

3.5. Total density computation

When all the accelerations shown above were calculated, it's possible to extract the drag acceleration by the following equation:

$$\vec{a}_{drag} = \vec{a}_{true} - (\vec{a}_{SR} + \vec{a}_{EA} + \vec{a}_{IR}) \tag{3-13}$$

where $\vec{a}_{true}$ is the acceleration measured by the accelerometers onboard and corrected by bias and scale factors, $\vec{a}_{SR}$ is the acceleration due to solar radiation pressure, $\vec{a}_{EA}$ and $\vec{a}_{IR}$ are, respectively, the accelerations due to the Earth albedo and infrared pressures.

Equation 3-7 must be used to calculate density, but before C_D and $\vec{v}_{rel}$ have to be defined. For C_D, equation 3-11 is utilized for panels inclined to the velocity vector, directed along the roll axis, while, for panels parallel to flow, equation 3-12 is used. Considering that, for GRACE mission, the molecular speed ratio varies between 5.4 and 9.7 [18].

Neglecting the velocity of any deviation in wind speed for this model, both to simplify the equations, because it's difficult to estimate wind speed a priori and requires another rather uncertain model, and because it's lower than spacecraft's speed when geomagnetic activity is low [19],

$$\vec{v}_{rel} = \vec{v}_{sc} - \vec{\omega}_E \times \vec{r} \tag{3-14}$$

where $\vec{v}_{sc}$ and $\vec{r}$ are GRACE velocity and position, respectively, obtained by GNV1B data and translated on the SRF and $\vec{\omega}_E$ is the Earth rotational velocity, assumed as constant. The adopted constant value for the Earth's rotation is $\vec{\omega}_E = 7.292115 \cdot 10^{-5} \pm 1.5 \cdot 10^{-12} rad/s$.

With these assumptions, equation 3-7 is solved for density using the along-track axis of the accelerometer, directed parallel to velocity vector, denoted by $\vec{a}_{drag} \cdot \hat{x}$, so:

$$\rho_{SuperSTAR} = -\frac{2m\left(\vec{a}_{drag} \cdot \hat{x}\right)}{\sum_{i=1}^{6}\{A_i C_{Di}[\vec{v}_{rel} \cdot \hat{n}_i]\vec{v}_{rel}\} \cdot \hat{x}} \tag{3-15}$$

In the following chapters, differences between density obtained by GRACE accelerometer and atmosphere model's one will be shown.

Chapter 4

Data and model evaluation

Until now, the study was about the way to calculate density. In this chapter the results obtained both from atmospheres model and from directed accelerations data will be shown to realize a comparison for each period considered.

4.1. Density from atmospheres model

Considering the comparisons between the models shown in chapter one, the most accurate seems to be the J-71, but, as it was said, data presented in tab 1.2 must consider the uncertainty of the drag coefficient of 15%. Moreover, those values are for satellites of particular shape and don't cover heights of GRACE satellite and all possible solar flux. For these reasons and for the similarity between MSISE-90 and NRLMSISE-00 under GRACE operative conditions, the MSISE-90 model was chosen for the purpose of this thesis. Actually, another reason of this choice was the availability of the model for MATLAB software approved and upgraded by Community Coordinated Modeling Center (CCMC).

The inputs for MSISE-90 model (see Appendix 1), for the cases presented, are:

- Time: one point each ten minutes from the midnight of the 1st August 2002 to the midnight of the 28th of August 2002; from the midnight of the 1st June 2008 to the midnight of the 1st of July 2008; from the midnight of the 1st June 2012 to the midnight of the 1st of July 2012.
- Latitude, longitude and altitude: GPS navigation data provide the position of the satellite in the Terrestrial frame; after that, with the MATLAB routine "ecef2lla", it is possible to convert Earth-Centered Earth-Fixed (ECEF) coordinates to geodetic ones.
- $F_{10.7}$ daily: this value represents the incoming solar radiation and, as it is possible to see in the figure 4.1, there are several differences among the three periods. Indeed, in 2002, immediately after the beginning of the mission there was a maximum solar flux. Because the mission covers a complete 11-years solar cycle, in 2008 there was a minimum solar flux, while in 2012 it was moderate. Consequently, each possible condition of solar activity is considered.
- $\bar{F}_{10.7}$ 3-month average: it is the value averaged over 3 months of $F_{10.7}$ daily data.

- A_p daily: it provides the information about the geomagnetic activity below the auroral zones. Figure 4.1 shows that, during all the periods of time considered, the geomagnetic activity was rather low, being always under 50 gamma.

Both $F_{10.7}$ daily, $\bar{F}_{10.7}$ 3-month average and A_p daily data were provided by the Community Coordinated Modeling Center (CCMO) of NASA.

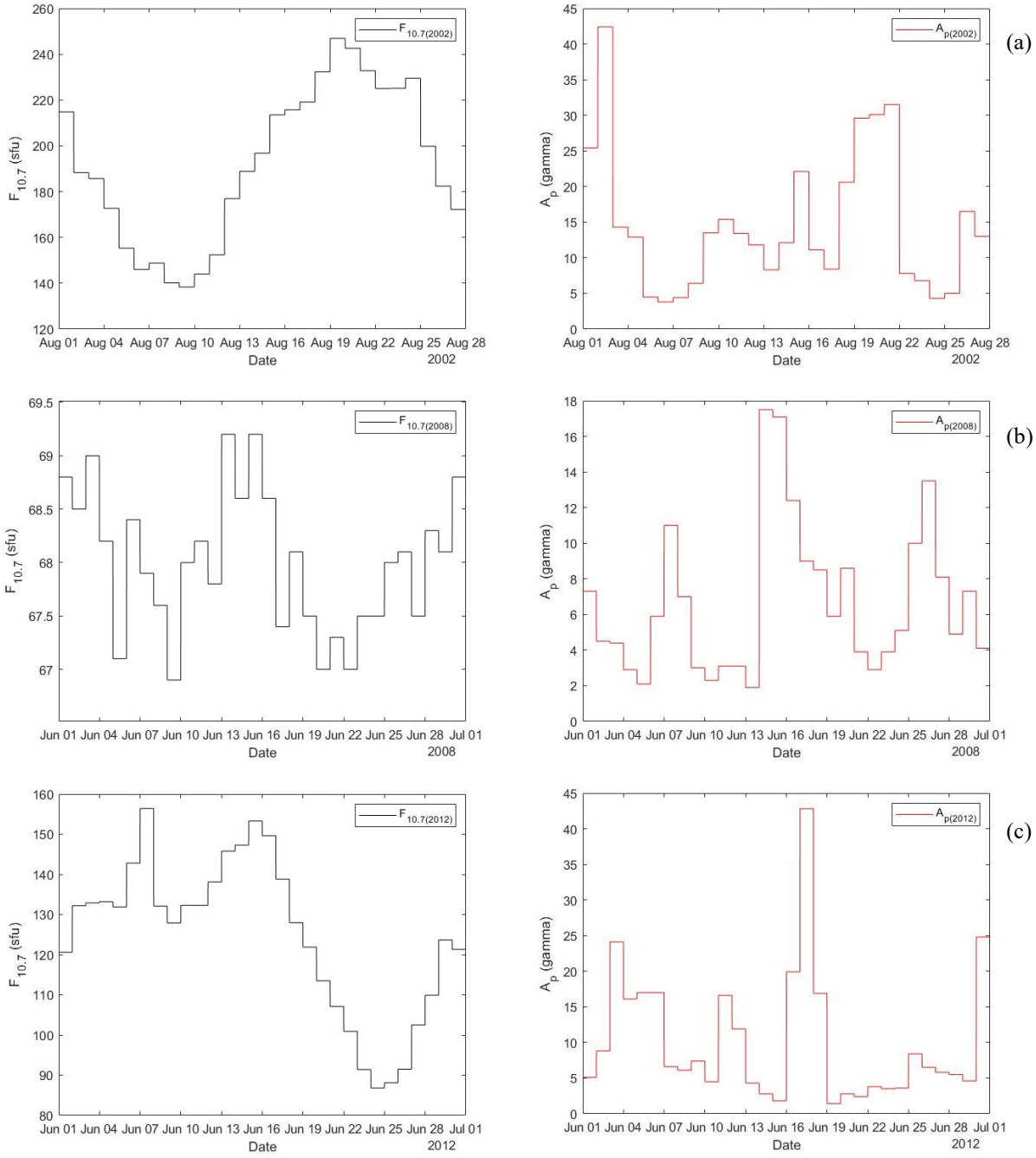

Figure 4.1: $F_{10.7}$ and A_p for August 2002, high solar activity(a), June 2008, low solar activity(b), June 2012, moderate solar activity(c)

The outputs of the model are the neutral and exospheric temperature, the number density of all the species present in the atmosphere (O, N2, O2, He, Ar, H, N) and the value of the total mass density.

The values of total density got by the MSISE-90 model, for each period, are shown in figure 4.2. It's evident that densities trends are influenced by both $F_{10.7}$ and A_p. Indeed, the trends follow the ones of $F_{10.7}$, but the maxima are when the magnetic activity increases. For example, in 2012 the A_p has a maximum value between 16th and 19th of June and the density has a corresponding maximum during those days.

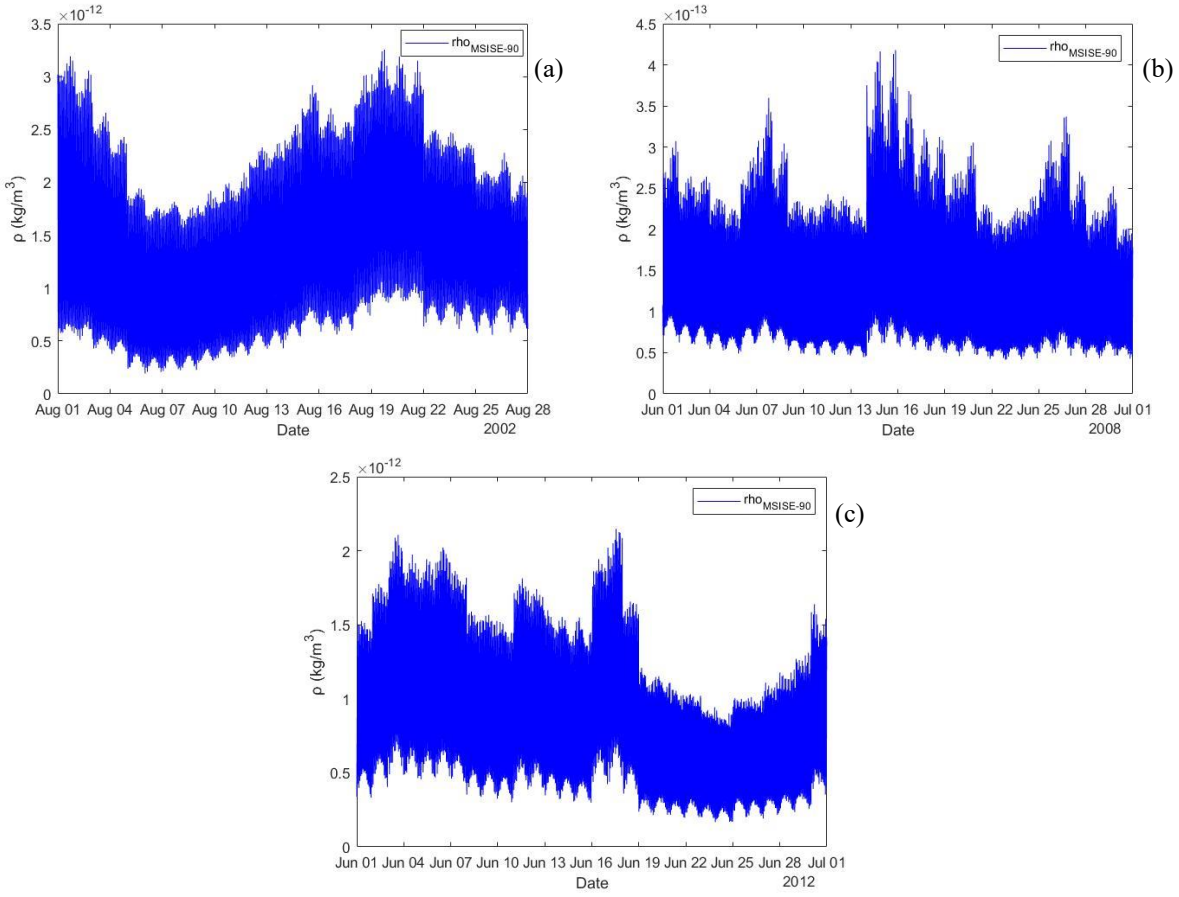

Figure 4.2: density values obtained from MSISE-90 model for August 2002, high solar activity(a), June 2008, low solar activity(b), June 2012, moderate solar activity(c)

4.2. Density from accelerations data

Density is extracted from the accelerations data with the procedure described in the previous chapter. At the end, the density is obtained from the drag accelerations acting on the along-track, the axis directed parallel to the direction of the velocity, of the GRACE-A spacecraft, by the equation 3-15.

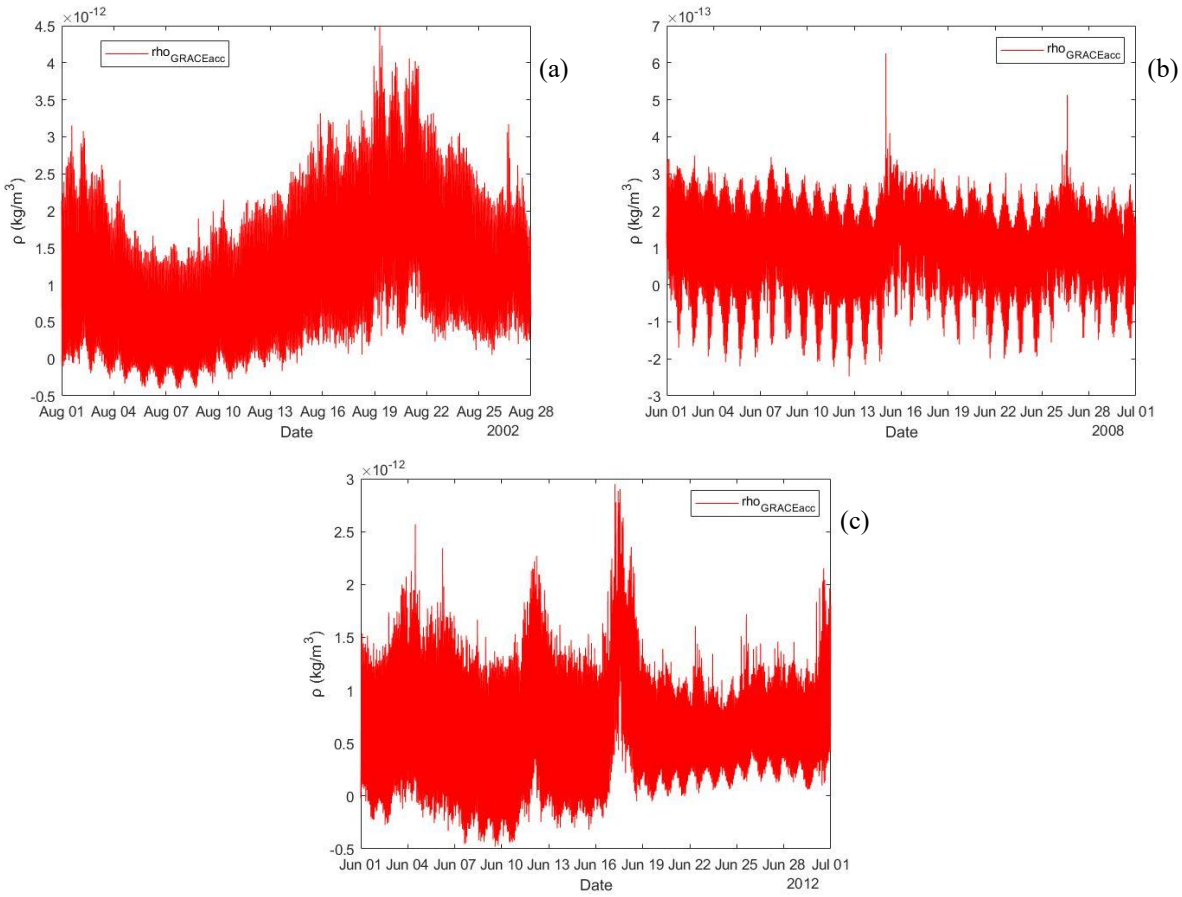

Figure 4.3: density values obtained from SuperSTAR accelerometer of GRACE-A for August 2002, high solar activity(a), June 2008, low solar activity(b), June 2012, moderate solar activity(c)

Figure 4.3 shows the values of density obtained by the accelerations data. The trend is always similar to those of F10.7 and Ap index, therefore, the dependence from the solar irradiance and geomagnetic activity is confirmed. The presence of some negative values may be due to the sources of error present in the various phases of the model. First of all, the noise of the accelerometer instruments that bias and scale have decreased, but they certainly don't have totally eliminated because they are based into a mathematical equation that should be evaluated for each considered time lapse of the mission. Secondly, the modeling of each force, that introduces an error caused by the geometric simplification and the absence of information about the state of the spacecraft surfaces properties that have a decay during the mission. In particular, for the modeling of the albedo and infrared radiation pressures, the quantities of solar radiation reflecting by the Earth and infrared energy emanating at the Earth's surface are considered as an average over the entire Earth's surface, because the model doesn't consider if the satellite was over ocean, where, for example, the coefficient of albedo is almost zero, or over the poles, where it is close to the unit. Further errors are introduced by the drag acceleration equation:

$$\vec{a}_{drag} = -\frac{C_D A}{2m}\,\rho {v_{rel}}^2 \frac{\vec{v}_{rel}}{|\vec{v}_{rel}|} \tag{4-1}$$

Indeed, it's necessary to know the values of the drag coefficient, C_D, because, otherwise the equation 4-1 would have two unknowns and it would be undetermined. The Cook's formula [15], used for this purpose, is anyway a model and, therefore, introduces an error. Even the $\vec{v}_{rel}$ contains an error because the deviations of the wind speed have been neglected with respect the velocity of the satellite.

4.3. Data comparison

Before doing the comparison, because of the large amount of data and the errors present especially in accelerometers data, it's necessary to filter and smooth all data. The MATLAB toolbox "Signal Analyzer" was used to realize this process [31]. First of all, data were filtered with a lowpass filter to eliminate the frequencies too high which produced noise for the instruments. Afterwards, a Savitzky-Golay filter was used to smooth data and give the opportunity to do a realistic comparison.

Once this process is completed, it is possible to compare density of MSISE-90 model with the one obtained by SuperSTAR accelerometer onboard of GRACE, as shown in figure 4.4.

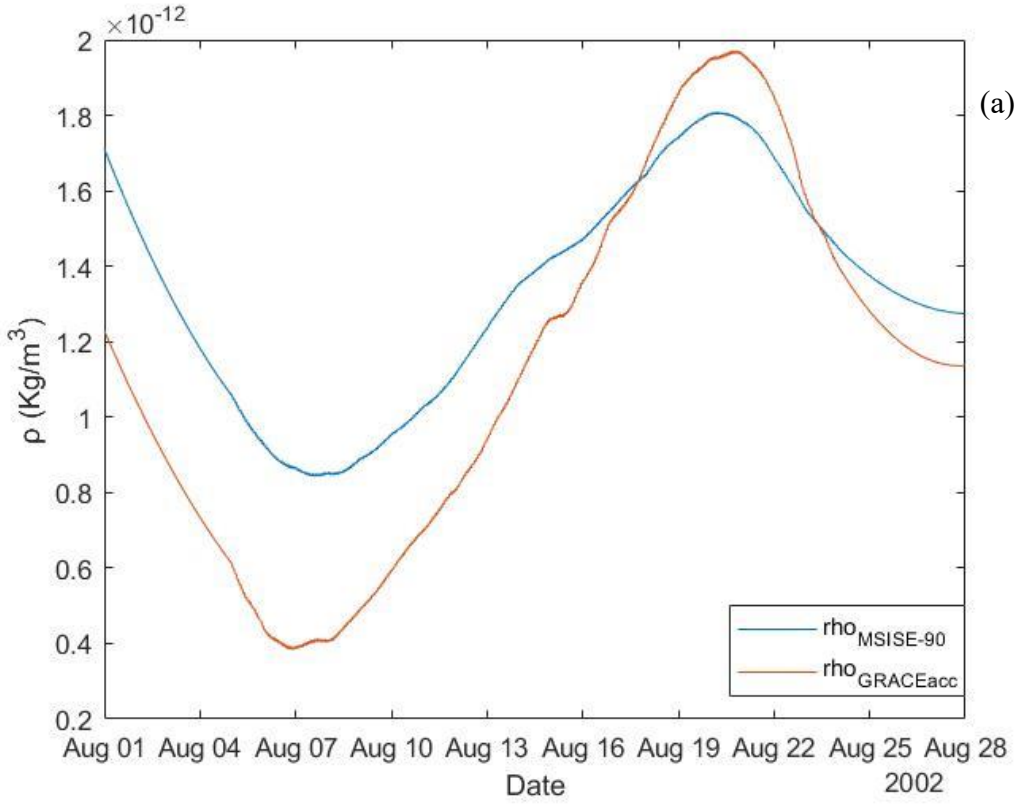

(a)

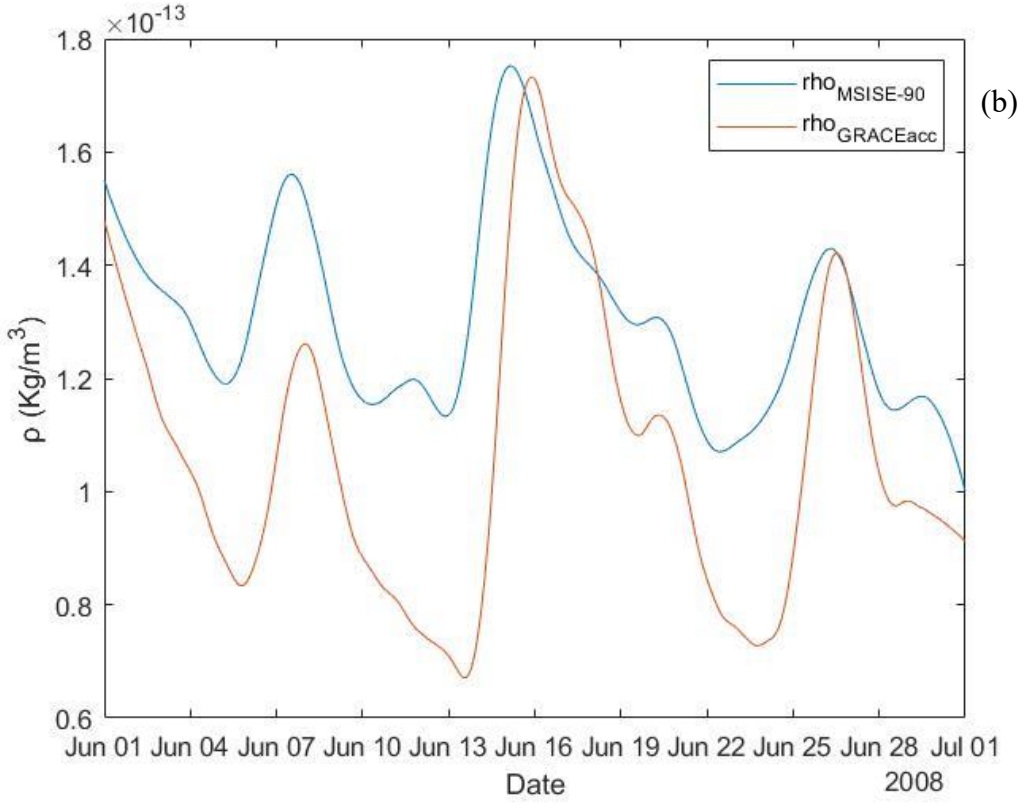

(b)

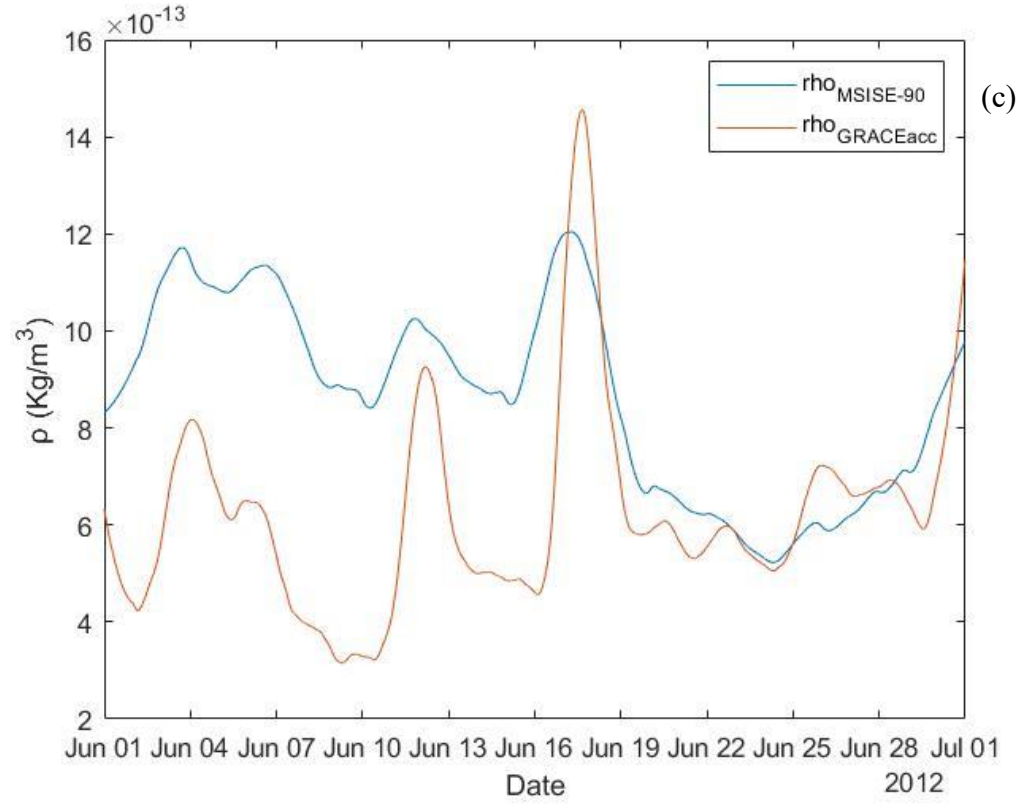

(c)

Figure 4.4: comparison between density obtained by MSISE-90 model and GRACE accelerometer. (a) high solar activity, (b) low solar activity, (c) moderate solar activity

Some considerations can be done, about the comparison:

- Density computed by MSISE-90 model is, on average, higher than the one obtained by the GRACE accelerator data at all solar conditions. This means that MSISE-90 model overestimates the real data, according to the results collected in table 1.3. However, for the conditions of high and moderate solar activity, where there is a noticeable variability of $F_{10.7}$ and A_p, the values of MSISE-90 are lower near the high peaks.
- For each period of time considered there is an offset between the peaks of two kinds of data. This is due to the filtering of data which can't be extremely accurate because the many sources of noise and the few points for each orbit. Indeed, if it was considered a point for each second for an entire orbit, the trend of the graph should be less jagged.
- Figure 4.5 shows that the differences between the two set of data don't exceed 60% for the high and low solar activity and are low over 60% for the moderate solar activity during the first half of the month. These discrepancies are quite high relative to previous studies which present variations around 20% [13][19][20] with peaks up to 30% [14] and, surely, might be reduced refining accelerometer data from errors presented above, improving the filtering and implementing models of perturbative accelerations and geometry.

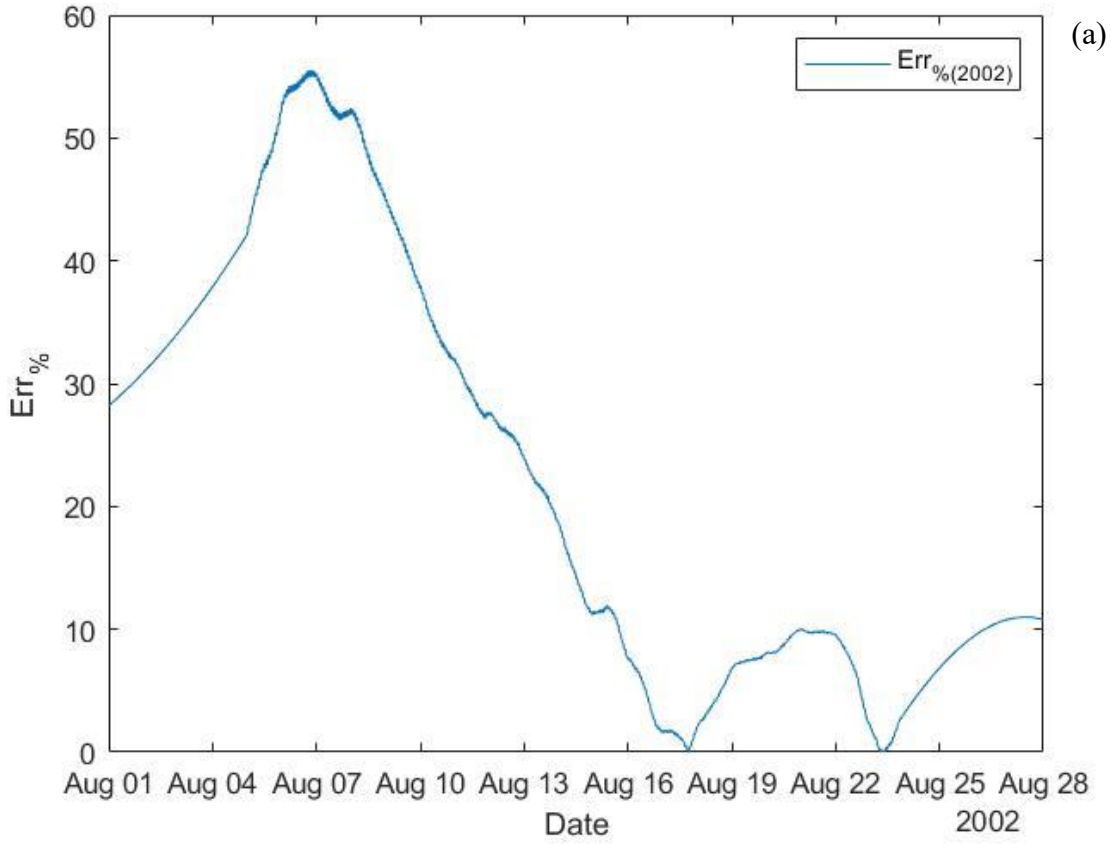

(a)

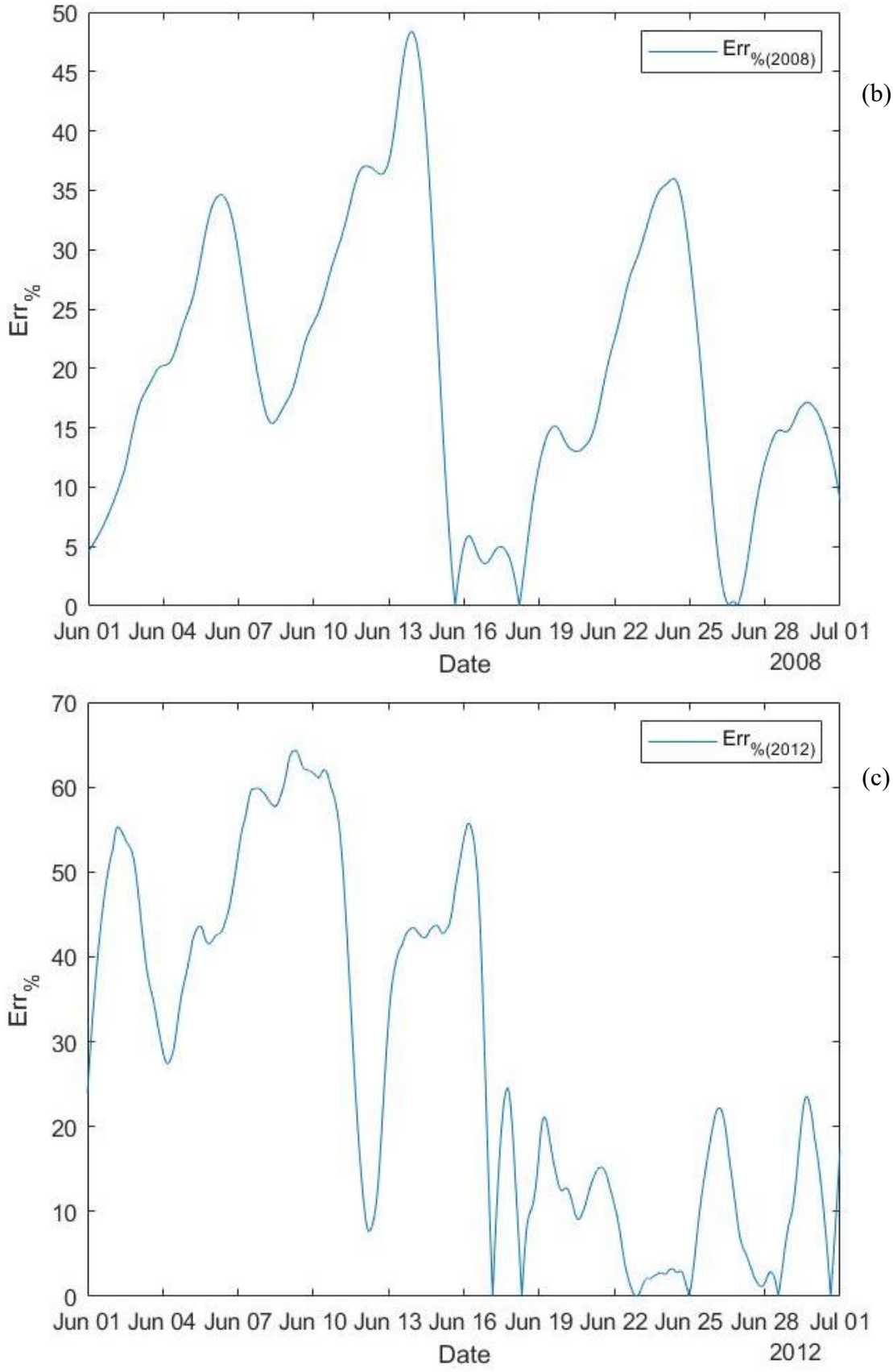

Figure 4.5: percentage error between density calculated with MSISE-90 model and the one obtained by GRACE-A accelerometer data at (a) high, (b) low, (c) moderate solar activity

The results indicate that the GRACE accelerometer data provide an important measurement for improvement in modeling of density variations at GRACE altitudes.

Chapter 5

Future applications: METRIC

As shown in the previous chapter, all satellites that carried accelerometers on-board hadn't the scientific objective to measure atmospheric density, but they used accelerations measured to improve their study about gravitational field. In this chapter, Measurement of EnvironmenTal and Relativistic In-orbit preCessions (METRIC), a possible satellite that have, among main objectives, measuring atmospheric density one, will be presented [21].

5.1. Mission overview

Measurement of EnvironmenTal and Relativistic In-orbit preCessions (METRIC) is a concept to make use of existing technology developed for acceleration measurement in space and state-of-the-art satellite tracking to precisely determine the orbit of a spacecraft with well-defined geometrical and mass characteristics and to measure over a long period of time the drag deceleration (as well as other non-gravitational perturbations) acting on it. This will result in a virtually drag-free spacecraft that can be exploited to investigate several effects related to gravitational physics and to the near-Earth environment, via a precise analysis of its orbital dynamics. Consequently, this mission would complement previous geodynamic and atmospheric ones in providing data useful to constrain competitive models of the gravitational interaction, as well as those related to atmospheric drag.

The accelerations that METRIC would measure during its orbit, would be used in two different ways. While for gravitational and geodynamic studies, accelerations need to measure a noise that can bias the parameters' estimate, for the atmospheric environment, they need to extract atmospheric drag and then density. A 450x1200 km high-inclination orbit would enable the sampling of an important circumterrestrial region to improve the knowledge of neutral atmospheric density that would be relevant for both space operations and science. The altitude range considered is characterized by a compositional and density landscape strongly affected by the time-varying solar activity. Unlike previous estimates of atmospheric density (obtained from satellite orbital decay and therefore being averages over many orbits), the on-board accelerometer will allow instantaneous measurements over the altitude range of interest.

A satellite like METRIC may be considered in the middle between LAGEOS and GRACE. The former (along with its twin LAGEOS II and the recently-launched LARES) is a good example of an object developed, built and launched to work as a gravitational test mass. It is

completely passive (no instrumentation or any devices on-board); therefore, any dynamical perturbing effect acting on it should be a-posteriori modeled, either analytically or numerically. In GRACE, the effects of non-gravitational origin are directly measured by a three-axis accelerometer, made necessary by the need to remove the combined contributions of non-gravitational perturbations from the satellite-to-satellite tracking data, of which the air-drag is the dominant effect at the orbital altitude of GRACE The proposed mission retains the basic idea of having an object of a simple shape, including a three-axis accelerometer package in order to overcome the problems related to modeling the non-gravitational effects and, at the same time, separating the air-drag from the solar-pressure effects.

The orbit of Metric is an elliptical (eccentricity 0.052), dawn-dusk and Sun-synchronous one and altitude ranges between 450 km and 1200 km. Adopting this orbital configuration, when the satellite is at the apogee the predominant nongravitational force is the solar radiation pressure and therefore all the accelerations measured by the accelerometer are due to it. Because these accelerations have the same order of magnitude during all the METRIC orbit, the drag ones can be extract with more accuracy at lower heights where, instead, the air drag accelerations are about two orders of magnitude stronger.

The spacecraft has a very simplified geometry; indeed, it should be a sphere of radius 1 m and spinning about its longitudinal z-axis that will be orthogonal to the orbital plane. Choosing this geometry, it's not necessary to divide the satellite into different panels but, according to the nongravitational force that one is modelling, the cross-sectional area is always the same and the normal unite vector is the one directed towards the source. The spin about an axis close to orthogonal to the orbit plane provides the basic attitude stabilization of the spacecraft to be occasionally adjusted by the attitude control system. Another important feature deriving from the choice of geometry is that the surface of METRIC is covered by solar panels.

The body reference frame for this satellite is the Satellite Coordinate System one that it moves with the satellite. The x axis points always from the Earth's center along the radius vector to the satellite as it moves through the orbit; the z axis is fixed along the direction normal to the orbital plane; the y axis is along the direction of the velocity vector and is perpendicular to the radius vector. Radial positions and displacements are normal to the position vector (along the x axis), along-track displacements are normal to position vector (along the y axis) and cross-track positions are normal to the plane defined by the current position and velocity vectors.

The spacecraft should also carry all the necessary subsystems for the satellite functions, inclusive of the attitude determination and control, through magneto torquers, of the spin axis orientation. Spin could be initiated by the release mechanism at ejection from the rocket stage and later fine-tuned with the magneto torquers. Telecommunication with the ground will be guaranteed via an S- or X-band link, which would provide also basic tracking capabilities.

Enhanced tracking will be obtained by equipping the spacecraft with a global navigation satellite system (GNSS) receiver. High-precision spacecraft orbit determination will be made possible by equipping it with a set of retroreflectors for laser ranging from the International Laser Ranging Service (ILRS) stations. The baseline for the mission is a minimal duration of

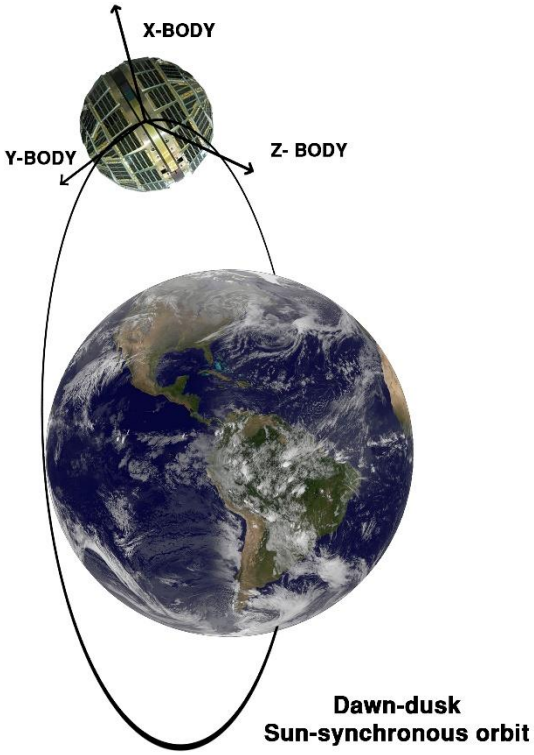

Figure 5.1: schematic of the proposed METRIC spacecraft and orbit

2–3 years, with an extended mission phase possibly aiming for a full solar cycle of 11 years.

In the following table the main characteristics for orbit and spacecraft properties are shown. For the following analysis, the surface properties are the same of the solar panel of GRACE. Obviously, the spacecraft model introduced here is a concept that might be modified after future studies.

Feature	Value/type
Spacecraft mass	100 kg
Spacecraft radius	1 m
Surface area	12.566 m^2
Semimajor axis	$7.2x10^6$ m
Eccentricity	0.052
Inclination	98.662°

Table 5.1: main features of the proposed configuration for METRIC []

5.2. Accelerometer

METRIC mission needs a very sensitive accelerometer because the expected accelerations directed along-track are of a magnitude of at least 10^{-7} - 10^{-8} m/s^2 according to accelerations measured from GRACE. Considering the state-of-the-art, the Italian Spring Accelerometer (ISA), shown in figure 5.2, could be a possible solution [22]. It's a three-axis, high-sensitivity accelerometer developed for space applications, but available also for ground uses. This device is actually on-board of BepiColombo spacecraft, launched the 20th October 2018 and it should reach Mercury on 2025. ISA consists of three one-dimensional sensing elements, one for each axis, disposed such that the sensing directions are orthogonal one another. Each sensing element is practically a one-dimensional harmonic oscillator, in which a sensing mass is connected to an external frame with a flexural spring; the entire system is obtained by the manufacturing of a single piece of aluminum. The central mass is between two pick-up plates to form a two-face capacitor. The two-face capacitor and the other two fixed ones are part of a capacitive bridge for signal read-out. An acceleration acting on the system (its component along the normal to the plates) induces a motion of the central mass and unbalances the bridge. The corresponding signal is then read out and properly amplified and filtered. The signals coming from each accelerometer element can therefore be combined to obtain the acceleration vector at a reference point of the accelerometer.

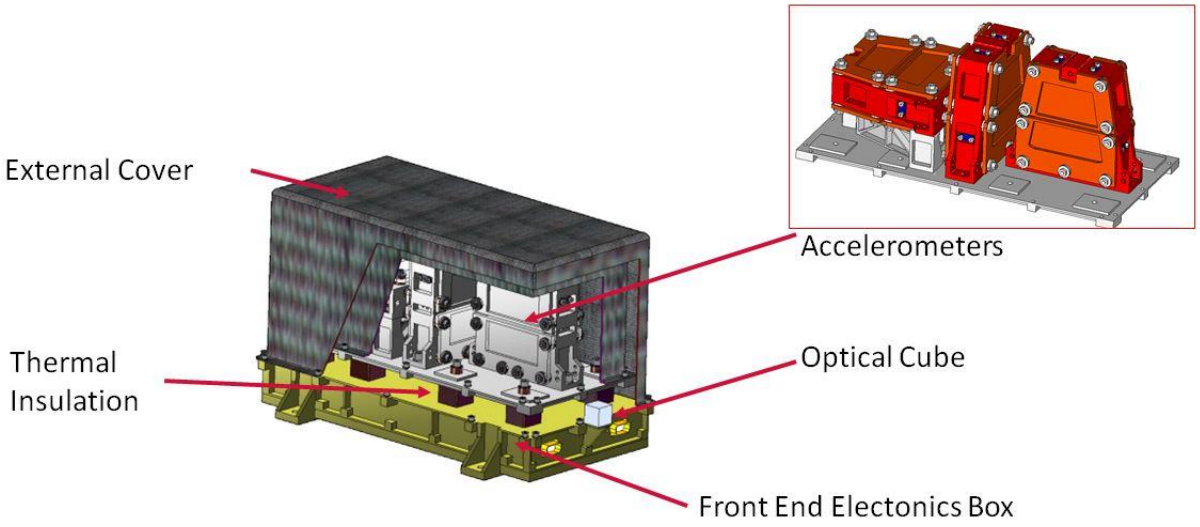

Figure 5.2: ISA accelerometer on-board of BepiColombo satellite [22]

The sensitivity of the ISA accelerometer is in the order of $10^{-9}\, m \cdot s^{-2} \cdot Hz^{-1/2}$. This level has been reached after a series of test on the ground over many accelerometer prototypes assembled in differential configuration, in a wide band of frequencies below 10^{-1} Hz. Each sensing element has another two plates able to give to the mass a known acceleration signal useful for internal calibration that can be enhanced with a posteriori bias. To avoid noise due to mechanical or thermal environment, the accelerometer package is positioned as close as possible to the satellite spin axis.

5.3. Non-gravitational forces modeling

The non-gravitational forces acting on METRIC, obviously, are the same of GRACE, but there are some differences due to the altitudes reach by METRIC and the strong geometric simplification. Indeed, because of the spherical shape of spacecraft, it's supposed that satellite is always facing the source (Sun for the solar pressure and Earth for albedo and infrared ones respectively) and, hence, the unite normal vector of METRIC surface is the unite normal vector directed towards the source in that moment and the area hit by the radiation is always a circle of unit radius .

To better investigate density variations during a complete Earth revolution around the Sun, four different times of the year 2017(spring and winter equinoxes, summer and winter solstices) have been taken into account. As it was said above, the hypothetical METRIC orbit is a Sun-synchronous dawn-dusk, however, during the study was considered also a noon-midnight orbit to evaluate different incidence angles of solar radiation pressure [25]. For all the cases at least 5 complete orbits of METRIC are considered.

5.3.1. Solar radiation pressure

The equation used to compute the accelerations relative to solar radiation pressure is the simplified form relative to the equation 3-1, because it is supposed that the surface normal $\hat{n}$ always points towards the Sun [23] [24]:

$$\vec{a}_{SR} = -\frac{RA}{mc} C_R k \hat{s} \tag{5-1}$$

where R is the incoming solar radiation flux [28], A is the exposed area of the satellite to the incoming radiation, m is the satellite's mass, c is the speed of light, C_R is the radiation pressure coefficient, k is the correction coefficient, in the general case is unitary, and $\hat{s}$ is the unite satellite-Sun vector. The C_R value varies between 0 and 2 and indicates how the satellite surfaces reflect the incoming radiation. If it's 0, the surface allows all light to pass throw and no force is transmitted; if it's 1, all the radiation is absorbed and all force is transmitted (black body); if it's 2, all the radiation is reflected and twice the force is transmitted to the surface. Because it may be supposed that METRIC is covered by solar panels, $C_R = 1.21$[24].

In this case, the ratio to account for how much incoming solar radiation hit the satellite isn't available and, therefore, it is necessary to analyze METRIC orbit to find when the satellite is hidden by the Earth. To this purpose the MATLAB algorithm SIGHT is used [23].

5.3.2. Albedo and infrared radiation pressures

The equation used to compute the accelerations relative to albedo and infrared radiation pressure are:

$$\vec{a}_{alb} = \frac{R_{alb} \cdot A \cdot C_a \cdot k}{mc} \sin^2(2\eta_{horizon})\,\hat{r} \tag{5-2}$$

$$\vec{a}_{ir} = \frac{IR \cdot A \cdot C_\varepsilon \cdot k}{mc} \sin^2(2\eta_{horizon})\,\hat{r} \tag{5-3}$$

where R_{alb} is the solar radiation reflected by the Earth that hit satellite, IR is the infrared energy emanating at the Earth's surface, A is the exposed area of the satellite to the incoming radiation, C_a and C_ε are the absorption and emissivity coefficients, respectively, of the satellite material, k is the correction coefficient, in the general case is unitary, $\eta_{horizon}$ is the angular radius of the Earth as seen for the satellite and $\hat{r}$ is the unite normal vector directed towards the Earth.

Both R_{alb} and IR are obtained by ERA5 [30], a climate reanalysis dataset, covering the period 1950 to present, developed through the Copernicus Climate Change Service (C3S). The name ERA5 refers to ECMWF Re-Analysis, with ERA5 being the fifth major global reanalysis produced by European Centre for Medium-range Weather Forecasts (ECMWF). ERA5, actually, provides data from 1979 to present for each hour of the day and with a horizontal resolution of 0.25°x0.25°. For the purposes of this thesis, the model proposed by ERA5 is simplified averaging data obtained over all the Earth's surface. This solution introduces an error, but greatly reduces the computation that would be obtained if the Earth were divided into grids.

5.3.3. Atmospheric drag

The equation used to compute the drag accelerations due to atmospheric drag is:

$$\vec{a}_{drag} = -\frac{C_D A}{2m}\,\rho {v_{rel}}^2 \frac{\vec{v}_{rel}}{|\vec{v}_{rel}|} \tag{5-4}$$

Where the C_D is the drag coefficient, A is the cross-sectional area, defined to be the area which is normal to the satellite's velocity vector, m is the satellite mass, ρ is the atmospheric density and v_{rel} is the velocity of the satellite with respect to the surrounding atmosphere.

Density is calculated by the model MSISE-90 (see Appendix 1) during the four different periods of time. The model provides density up to a height of 1000 km because after that altitude the magnitude decreases, and the drag acceleration become negligible. Figure 5.3 shows density for the spring equinox, it decreases from the perigee to the apogee and becomes null over 1000 km of altitude.

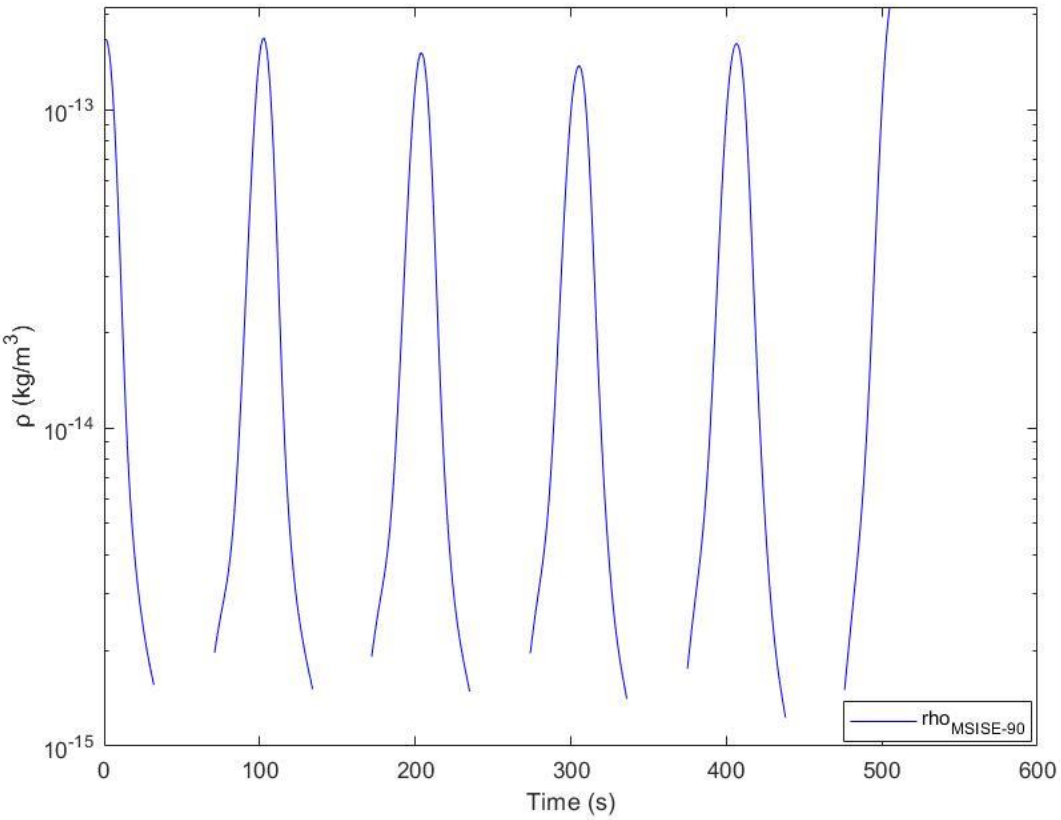

Figure 5.3: semilogarithmic graphic of density measured by MSISE-90 for the 21st of March 2017 (spring equinox) during 5 complete orbits.

To calculate C_D is used equation 3-10 where, not having the opportunity to know the temperature of the wall, it is set for 300 K [16]. To estimate v_{rel} is used equation 3-14, always neglecting the wind speed.

5.4. Density variations

After modeling all forces and, therefore, the accelerations, it is possible to have the total acceleration acting on the satellite:

$$\vec{a}_{total} = \vec{a}_{drag} + \vec{a}_{SR} + \vec{a}_{EA} + \vec{a}_{IR} \tag{5-5}$$

where $\vec{a}_{drag}$ is acceleration relative to drag, $\vec{a}_{SR}$ is acceleration relative to solar radiation pressure, $\vec{a}_{EA}$ and $\vec{a}_{IR}$ are acceleration relative albedo and infrared radiation pressures respectively.

If total acceleration is considered as the one that the ISA accelerometer may measure during the orbit, modifying some parameters of solar, albedo and infrared radiation pressures,

variations of drag accelerations are obtained and, therefore, density changes can be shown. In particular, the cases of maximum pressures and minimum ones will be taken into account.

The parameter that can be modified are:

- R_{alb}, the solar radiation reflected by the Earth that hit the satellite, and IR, the infrared energy emanating at the Earth's surface. These fluxes are computed as an average on all the Earth's surface because the knowledge of where the satellite exactly is above the Earth requires a level of modelling that is too refined for the purposes of this thesis. However, the albedo depends strongly on the surface that reflects the radiation and it can vary between 0.06 of the open oceans and 0.9 of the ice with snow [32] (see figure 5.4). Even the infrared radiation varies because when the Earth absorbs sunlight, it heats up and this heat radiates back into the space according to the surface that was hit. Consequently, for the following analysis, the maximum and the minimum values provided by the ERA5 data are taken into account.

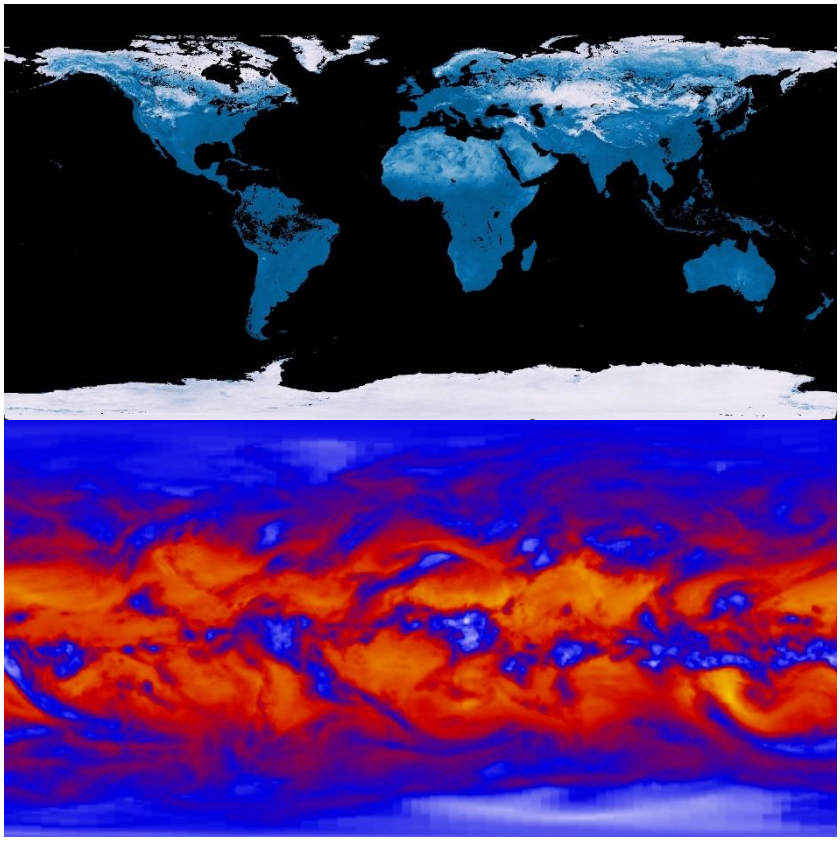

Figure 5.4: Albedo (a) and infrared radiation (b) on all the Earth surface. It's clear that values change depending on latitude and longitude. Credit: NEO

- The correction coefficient, k, that may be considered improved of 50% for the maximum case or halved for the minimum case, considering different kinds of materials or the possible deterioration during the mission. According to the equation 5-1, the solar

radiation pressure acceleration is directly proportional to the coefficient k and, so, the variations are of ±50% for the maximum and minimum cases.

Obviously, density variations occur below 1000 km of altitude and, especially, at the perigee, where the drag force is similar or higher than the solar radiation pressure, depending on the solar activity. So, considering the hypothetical Sun-synchronous dawn-dusk orbit, the solar radiation pressure acting along the axis parallel to the velocity vector is very small, because the solar flux is orthogonal to the orbit plane, as shown in figure 5.1. Consequently, the atmospheric drag acceleration at the perigee is somewhat higher than the SRP one. However, this configuration, even if it isn't suitable to evaluate the variations of density, may be very useful to measure the exact value of solar radiation pressure acceleration during all the METRIC orbit. Indeed, the acceleration measured by the accelerometer onboard above 1000 km is surely the value of solar radiation pressure one because the atmospheric drag is negligible, but also at lower altitudes, the data obtained along the z-axis, normal to the orbit plane, stand for the solar pressure because the drag is predominant along the y-axis while the albedo and infrared radiation are directed along the x-axis, the one which points towards the Earth.

To better evaluate possible density variations, the Sun-synchronous noon-midnight orbit was used, see figure 5.5. In this configuration, at the perigee, the SRP is directed parallel to the velocity vector and, hence, if it varies, the atmospheric drag acceleration changes because the total acceleration remains constant. Also in this case, the provision of albedo and Earth infrared radiation is negligible, because they are always directed along the radial axis pointing towards the Earth.

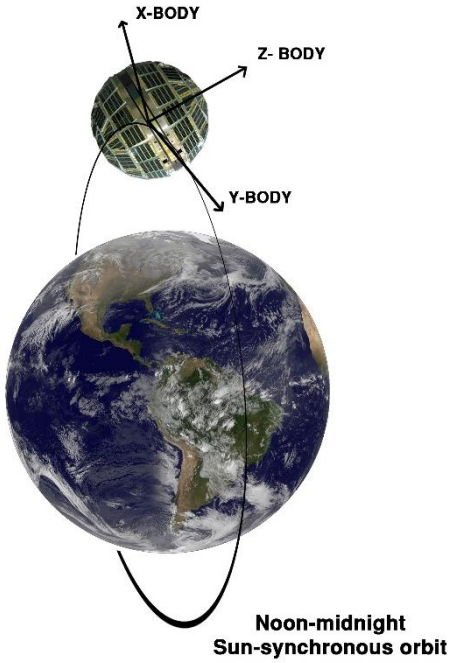

Figure 5.5: configuration used for better evaluate variations due to solar radiation pressure

The amplitudes of accelerations acting on the y-axis of METRIC at perigee obtained by the previous modeling of forces, are summarized in table 5.2. There are shown also $F_{10.7}$ and A_p. Because in 2017 the $F_{10.7}$ and A_p were low, the accelerations have the same order of magnitude even if drag accelerations are twice or three times bigger than the SRP ones. At the winter solstice the SRP acceleration isn't available because, at perigee, the satellite is in eclipse relative to the Sun. For this reason, this case is not considered in the following observations.

	$F_{10.7}$ (sfu)	A_p (gamma)	Drag accelerations (m/s^2)	SRP accelerations (m/s^2)
20/03/2017 (spring equinox)	70.5	1.4	$4.1 \cdot 10^{-7}$	$1.7 \cdot 10^{-7}$
21/06/2017 (summer solstice)	76.9	3.3	$3.4 \cdot 10^{-7}$	$1.6 \cdot 10^{-7}$
22/09/2017 (autumn equinox)	73.6	5.1	$5.6 \cdot 10^{-7}$	$1.7 \cdot 10^{-7}$
21/12/2017 (winter solstice)	71.8	2.1	$3 \cdot 10^{-7}$	NaN

Table 5.2: $F_{10.7}$, A_p and accelerations acting on the y-axis of METRIC, at the perigee, during equinoxes and solstices

Computed the SRP accelerations both at the maximum and minimum case, the equation 5-5 is used to calculate drag accelerations in the following way:

$$\vec{a}_{drag,max} = \vec{a}_{total} - \vec{a}_{SR,min} \tag{5-6}$$

$$\vec{a}_{drag,min} = \vec{a}_{total} - \vec{a}_{SR,max} \tag{5-7}$$

Where $\vec{a}_{total}$ is the total acceleration obtained in the average case, $\vec{a}_{SR,min}$ is the minimum solar radiation pressure acceleration and provides the maximum drag accelerations possible $\vec{a}_{drag,max}$. On the other side, $\vec{a}_{SR,max}$ is the maximum solar radiation pressure acceleration and provides the minimum drag accelerations possible $\vec{a}_{drag,min}$.

According to values of table 5.2, because the drag accelerations are twice or three times bigger than the SRP ones, the variations of ±50% of SRP accelerations cannot induce the same changes at the drag ones.

Once the drag accelerations for both cases are obtained, atmospheric drag can be extracted by the accelerations along the axis parallel to the velocity vector by the formula:

$$\rho_{max} = -\frac{2m\left(\vec{a}_{drag,max} \cdot \hat{y}\right)}{AC_D[\vec{v}_{rel} \cdot \hat{y}]^2} \tag{5-8}$$

$$\rho_{min} = -\frac{2m(\vec{a}_{drag,min} \cdot \hat{y})}{AC_D[\vec{v}_{rel} \cdot \hat{y}]^2} \tag{5-9}$$

where m is the mass of the spacecraft, A is the cross-sectional area, C_D is the coefficient of drag obtained by the equation 3-10, $\vec{v}_{rel}$ is the velocity of the satellite with respect to the surrounding atmosphere.

Figure 5.6 shows density discrepancies at the perigee between the average case and the maximum and minimum ones. In each of the periods of time considered, the variations of density are between ±20% and ±25%. Within these ranges, it's possible to take the value of atmospheric density to estimate the drag accelerations for the satellite orbit decay. The best choice of the value depends on the knowledge of the satellite geometry, the orbit configuration, the properties of the material surfaces and, consequently, how long the satellite is in the operating conditions. The case presented, is, maybe, the worst one because the two main accelerations have the same order of magnitude and the uncertainty of solar radiation coefficient is very high. However, this is a possible scenario, hence the possibility to launch METRIC should be very important, because, thanks to the accelerometers on-board coupled with its particular orbit, Sun-synchronous dawn-dusk, and shape, it may allow to compute a more precise atmospheric density, improve the existing density models and, therefore, decrease the uncertainty over coefficients, as the solar radiation one.

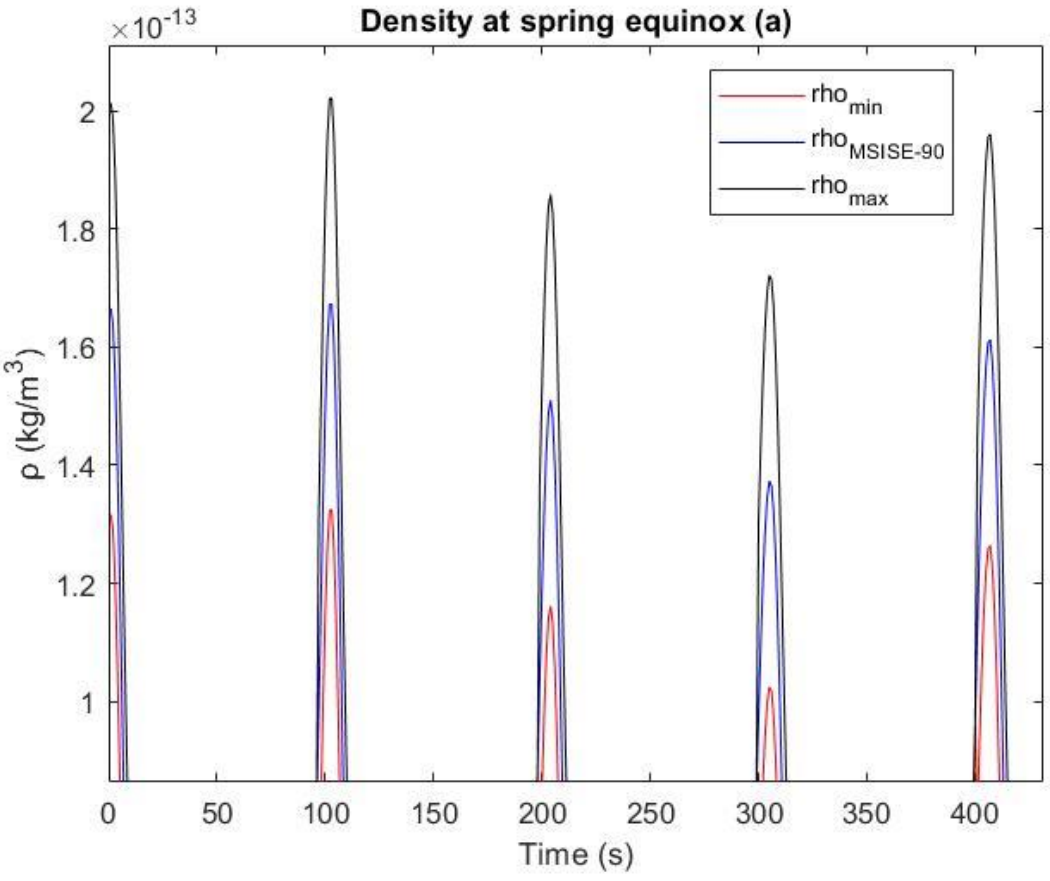

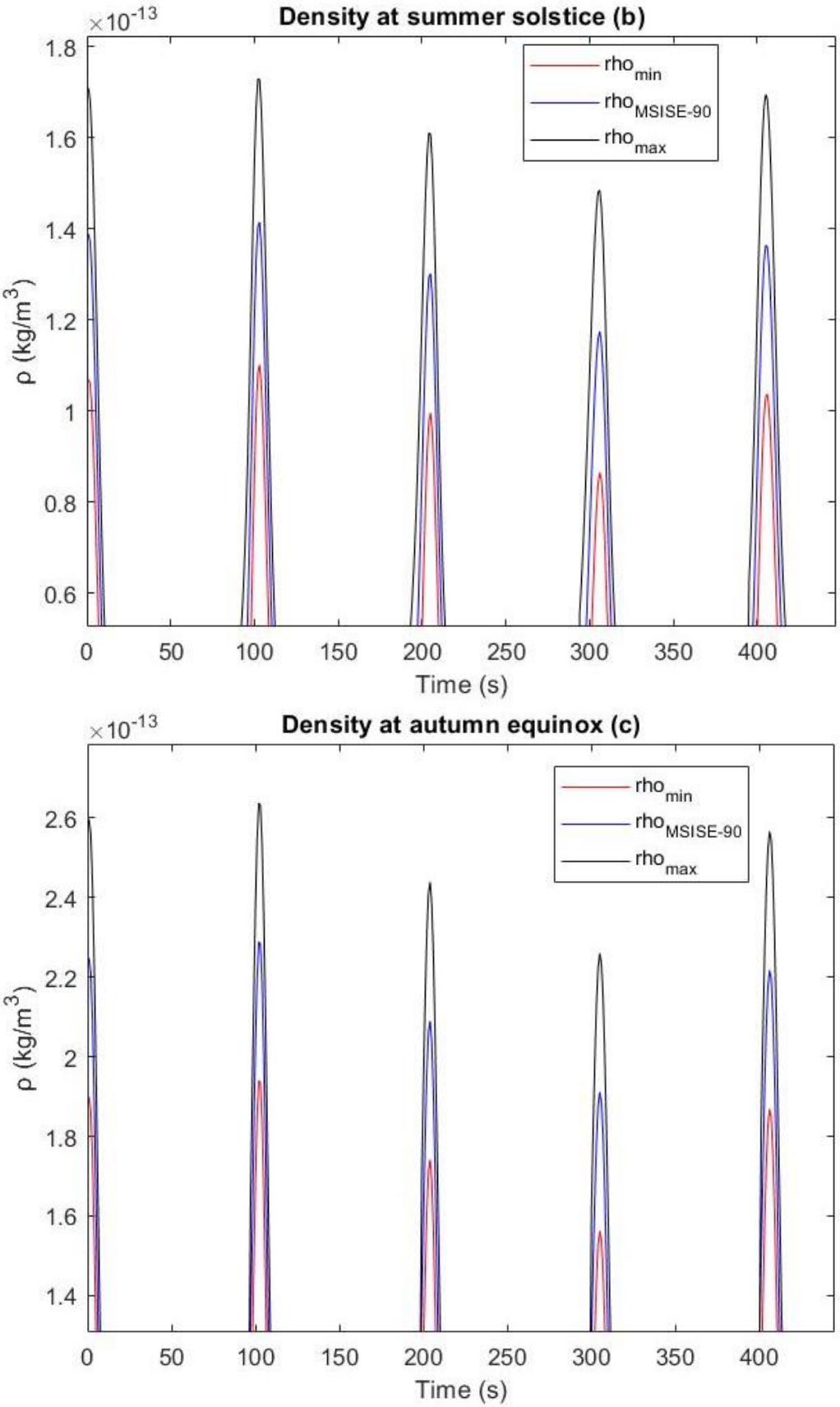

Figure 5.6: discrepancies, close to the perigee, between density calculated by the MSISE-90 and the one of maximum and minimum cases, obtained varying the radiation pressure coefficient of ±50% during the spring equinox (a), summer solstice (b) and autumn equinox (c)

5.5. Future improvements

The proposed modeling uses, for the drag accelerations, the equation 5-4, where in presence of GPS navigation data and knowing the geometry and the mass of the spacecraft, the unknowns are two: the density and the drag coefficient. For this thesis, the drag coefficient was modeled with the Cook's formula [15]:

$$C_D = 2\left[1 + \frac{2}{3}\sqrt{1 + \alpha\left(\frac{T_w}{V^2/(3R)} - 1\right)}\cos\theta\right] \tag{5-10}$$

where α is the energy accommodation coefficient, T_w is the wall temperature, V is the velocity of incident particles and θ is the angle of incident gas flow with to respect the satellite surface, but this procedure introduces an error.

To overcome the problem, one possible solution is that the spacecraft has on-board a pressure gauge [16]. In this way, it is possible to use the ideal gas law:

$$\frac{P}{\rho} = \frac{RT}{M} \tag{5-11}$$

where P, ρ and T are the pressure, the density and absolute temperature of the gas, R is the ideal gas constant and M is the molar mass. If the pressure gauge provides the instant pressure of the gas during the orbit and knowing the exospheric temperature by a temperature profiles of models, it's possible use the equation 5-4 to compute directly the density and, therefore, the equation of the drag accelerations may be used to extract the drag coefficient without modeling it a-priori.

Conclusions

Thesis has presented two different ways to calculate the atmospheric density: (a) the estimate from mathematical models and (b) the extraction from the total accelerations measured by accelerometers on-board of satellite. The total acceleration derives from all the forces acting on the surfaces of satellites and, in particular, those of atmospheric drag and solar pressure. An accurate knowledge of density is important to evaluate the drag force, that for low LEO orbit is the predominant force, and, hence, estimate with an appropriate precision the orbit decay. This is fundamental to know both the duration of the operative life of satellites, important from an economic and scientific point of view, and their real positions, important when new satellites must be launched in orbit. Indeed, one of the major problems on spatial environment is the presence of debris, also of big dimensions, not recorded.

Afterwards, a comparison between data calculated from the model MSISE-90 and ones obtained by extraction from the analysis of SuperSTAR accelerometer on-board of GRACE-A was done for each possible solar activity (low, moderate and high). In this thesis, the discrepancies found have been within accepted limits, and show that, at GRACE altitudes, the model overestimates the real data, confirming the results of previous studies. Hence, it would be important that more satellites had accelerometers on-board to have further data and, therefore, improve atmospheric models.

Considering results obtained, this thesis focused on METRIC, a proposed satellite, that has among its goals, the one of computing the accelerations to extract density. To better reach its purpose, the orbit of METRIC is the Sun-synchronous dawn-dusk one 450x1200 km of altitudes. Indeed, this configuration, at the apogee, calculates directly the acceleration due to solar, albedo and infrared radiation pressures that, at those heights, is two orders of magnitude higher than the drag one. This allows to have a landmark for lower altitudes because that value remains quite constant during the rest of the orbit, and, for a generic point of the orbit, if it is subtracted from the acceleration measured in that point, the drag acceleration is obtained without necessity of further modelling.

However, in this thesis a Sun-synchronous noon-midnight orbit was used to better underline the possible variation of the atmospheric density due to uncertainty of radiation pressure coefficient, because at the perigee, where SRP and drag accelerations have the same order of magnitude, SRP acting predominantly on the axis parallel to the velocity vector. The results, as expected, show that varying the SRP coefficient the estimated density changes. Consequently, the possibility to have a more accurate model allow to decrease the uncertainty on orbital propagation in LEO.

It should be noted that accelerometer measurements lead to the estimation of the product of density time the drag coefficient ($\rho \cdot C_D$). A possible future development to solve this problem is to add on-board a pressure gauge. Indeed, measuring pressure in combination with a temperature profile, the gas law allows to estimate separately the density and the drag coefficient.

It would be useful to conduct further studies to improve both the geometric and the force model for the satellites presented in this thesis, but also, design a formation of satellites of small size with accelerometers on-board to investigate density atmospheric at different altitudes of the atmosphere and collect more data to refine the atmospheric density models.

Nomenclature

ESA = European Space Agency

GRACE = Gravity Recovery And Climate Experiment

LEO = Low Earth Orbit

METRIC = Measurement of EnvironmenTal and Relativistic In-orbit preCessions

MSIS = Mass Spectrometer - Incoherent Scatter

NASA = National Aeronautics and Space Association

NEO = NASA Earth Observation

NOAA = National Oceanic and Atmospheric Administration

ρ = atmospheric density

ω = Earth rotational velocity

a = acceleration

A = area

A_p = planetary geomagnetic index

m = spacecraft mass

c = speed of light

C_D = drag coefficient

C_R = radiation pressure coefficient

c_r = reflectivity coefficient

$F_{10.7}$ = solar flux proxy

T = temperature

V,v = velocity

Bibliography

Papers/Articles/Reports

[1] D. A. Vallado, D. Finkleman (2014). A Critical Assessment of Satellite Drag and Atmospheric Density Modeling, *Acta Astronautica*, Vol. 95, February-March 2014, pp. 141-165

[2] W. K. Tobinska, T. Woods, F. Eparvier, R. Viereck, L. Floyd, D. Bouwer, G. Rottman, O. R. White (2000). The SOLAR2000 Empirical Solar Irradiance Model and Forecast Tool, *Journal of Atmospheric and Solar-Terrestrial Physics*, Vol. 62, pp. 1233-1250

[3] C. Pardini, W. K. Tobiska, L. Anselmo (2006). Analysis of the orbital decay of spherical satellites using different solar flux proxies and atmospheric density models, *Advances in Space Research*, Vol. 37, Issue 2, pp. 392-400

[4] A. E. Hedin (1987). MSIS-86 thermospheric model, *Journal of Geophysical Research*, Vol. 92, No. A5, pp. 4649-4662, May 1, 1987

[5] A. E. Hedin (1991). Extension of the MSIS Thermosphere Model into the middle and lower atmosphere, *Journal of Geophysical Research*, Vol. 96, No. A2, pp. 1159-1172, February 1, 1991

[6] J. M. Picone, A. E. Hedin, D. P. Drob, A. C. Aikin (2002). NRLMSISE-00 empirical model of the atmosphere: Statistical comparisons and scientific issues, *Journal of Geophysical Research*, Vol. 107, No. A12, pp. 1468, May 1, pp. SIA 15-1- SIA 15-16, December 2002

[7] G. M. Keating, J. C. Leary, B. D. Green, O. M. Uy, R. C. Benson, R. E., Erlandson, T. E. Phillips, J. C. Lesho, and M. T. Boies (1998). Neutral and ion drag effects near the exobase: MSX satellite measurements of He and O+, *Astrodynamics 1997: Advances in the Astronautical Sciences*, vol. 97(1), pp. 549– 556.

[8] C. Pardini, L. Anselmo (2001). Comparison and Accuracy Assessment of Semi-Empirical Atmosphere Models through the Orbital Decay of Spherical Satellites, *The Journal of the Astronautical Sciences*, Vol. 49, No. 2, April-June 2001, pp. 255-268

[9] NASA (2002). GRACE Launch press kit

[10] K. Case, G. Kruizinga, S. C. Wu (2010). GRACE Level 1-B Data Product User Handbook, JPL Publication D-22027

[11] S.V. Bettadpur (2007). GRACE 327-720 (CSR-GR-03-02) Gravity recovery and climate experiment product specification document (Rev 4.5, February 20, 2007), Center for Space Research, the University of Texas at Austin

[12] S.V. Bettadpur (2009). Recommendation for a-priori Bias & Scale Parameters for Level-1B ACC Data (Version 2), GRACE TN-02

[13] B. D. Tapley, J. C. Ries, S. Bettadpur, M. Cheng (2007). Neutral Density Measurements from the Gravity Recovery and Climate Experiments Accelerometers, *Journal of Spacecraft and Rockets*, Vol. 44, No. 6, November-December 2007, pp. 1220-1225

[14] E. K. Sutton, R. S. Nerem, J. M. Forbes (2007). Density and Winds in the Thermosphere Deduced from Accelerometer Data, *Journal of Spacecraft and Rockets*, Vol. 44, No. 6, November-December 2007, pp. 1210-1219

[15] K. Moe, M. M. Moe, C. J. Rice (2004). Simultaneous Analysis of Multi-Instrument Satellite Measurements of Atmospheric Density, *Journal of Spacecraft and Rockets*, Vol. 41, No. 5, September-October 2004, pp. 849-853

[16] K. Moe, M. M. Moe (2006). Method for deriving Densities and In-track Winds During Storms, *AIAA/AAS Astrodynamics Specialist Conference and Exhibit*, Keystone, Colorado, 21-24 August 2006

[17] G.E. Cook (1965). Satellite drag coefficients, *Planetary and Space Science*, Vol. 13, pp. 929-946

[18] G. Koppenwallner (2008). Comment on Special Section: New Perspectives on the Satellite Drag Enviroments of Earth, Mars and Venus, *Journal of Spacecraft and Rockets*, Vol. 45, No. 6, November-December 2008, pp. 1324-1327

[19] S. Bruinsma and R. Biancale (2003). Total Densities Derived from Accelerometer Data, *Journal of Spacecraft and Rockets*, Vol. 40, No. 2, March-April 2003, pp. 230-236

[20] C. A. McLaughlin, A. Hiatt, T. Lechtenberg (2011). Precision Orbit Derived Total Densities, *Journal of Spacecraft and Rockets*, Vol. 48, No. 1, January-February 2011, pp. 166-174

[21] R. Peron, E. C. Lorenzini (2017). METRIC: A Dedicated Earth-Orbiting Spacecraft for Investigating Gravitational Physics and the Space Environment, *Aerospace*, Vol. 4, 38

[22] V. Iafolla, E. Fiorenza, C. Lefevre, S. Nozzoli, R. Peron, A. Reale, F. Santoli (2011). The ISA Accelerometer for BepiColombo mission, *Memorie della Società Astronomica Italiana Supplementi*, Vol. 16, pp. 22-34

Books

[23] D. A. Vallado (2001). *Fundamentals of Astrodynamics and Applications* – Second Edition, Space Technology Library

[24] O. Montenbruck, E. Gill (2000), *Satellite Orbits: Models, Methods and Applications* - First Edition, Springer

[25] H.D. Curtis (2009). *Orbital Mechanics for Engineering Students* – Second Edition, Butterworth-Heinemann

Websites

[26] podaac-tools.jpl.nasa.gov/drive/files/GeodeticsGravity/grace

[27] www.ngdc.noaa.gov/stp/solar/solarirrad.html#composite

[28] lasp.colorado.edu/home/sorce/data/tsi-data/#data_files

[29] ssd.jpl.nasa.gov/horizons.cgi

[30] cds.climate.copernicus.eu/cdsapp#!/dataset/reanalysis-era5-pressure-levels?tab=overview

[31] it.mathworks.com/products/signal.html

[32] nsidc.org/cryosphere/seaice/processes/albedo.html

Appendix

1. Msis-E-90 script

```
function [density, temperature, f_10_7_used, Ap_used] = msis(time, ...
    latitude, longitude, altitude, utc, coord, curldir, f_10_7_daily, ...
    f_10_7_3month, ap_daily)

% MSIS Atmosphere model MSIS-E-90.
%
% Usage: [DENSITY, TEMPERATURE, F10_7_USED, AP_USED] = MSIS(TIME, LATITUDE,
%             LONGITUDE, ALTITUDE, UTC, COORD, CURLDIR, F10_7_DAILY,
%             F10_7_3MONTH, AP_DAILY)
%
% Computes the MSIS-E-90 Atmosphere Model, which is a model for Earth's
% atmosphere from the ground into the exosphere. MSIS stands for Mass
% Spectrometer and Incoherent Scatter Radar, which are the two data sources
% used to develop the model. The position and time inputs can be scalars or
% arrays; when they are arrays, they should all have the same number of
% elements. The outputs will be arrays with the same number of rows as
% elements in the input arrays, possibly 1 (so the shape of the input is
% not preserved).
%
% The function makes the computation by querying the online interface at
% https://ccmc.gsfc.nasa.gov/cgi-bin/modelweb/models/vitmo_model.cgi
% (hence internet access is required), which makes it pretty slow,
% especially when either more than one of the positions and time inputs are
% made to vary or if the position and time inputs are not spaced linearly.
% If more than one input is varied, the function can be sped up by using a
% for loop and holding the smaller arrays constant, assuming the largest
% array is spaced linearly. This will result in fewer calls to the website
% since the website allows for a linear sweep in one variable. See the
% script msistest.m for an example of this. There is one exception: The
% online interface has odd behavior that does not allow for sweeps in
% longitude for any altitude except the default (100 km), so longitude
% sweeps will be computed one at a time unless ALTITUDE is 100.
%
%
% The query is made using the command curl in an operating system terminal.
% This is built-in to Unix but not Windows. curl for Windows can be
% downloaded from http://curl.haxx.se/download.html. The directory where
% the curl.exe file can be found should be passed into CURLDIR for Windows
% computers. CURLDIR defaults to the same directory as this function.
%
% A value for -1 means the output is invalid for the given input.
%
% This is NOT the most recent MSIS model. The website for that version is:
%             http://www.nrl.navy.mil/research/nrl-review/2003/atmospheric-
science/picone/
%
% Inputs:
%   -TIME: Times to compute MSIS model either in MATLAB serial date number
%   format or a string that can be converted into MATLAB serial date number
%   format using DATENUM with no format specified (see documentation of
```

```
%   DATENUM for more information). Whether the times are local or UTC are
%   determined by the input UTC. Valid range is from year 1958 to year 2013
%   currently (optional, default is January 1, 2000 at 01:30).
%   -LATITUDE: Latitude in degrees to compute MSIS model. Whether this is
%   geodetic, geocentric, or geomagnetic latitude is determined by the
%   input COORD. Valid range is -90 degrees to 90 degrees (optional,
%   default is 50 degrees).
%   -LONGITUDE: Longitude in degrees to compute MSIS model. Whether this is
%   geodetic, geocentric, or geomagnetic longitude is determined by the
%   input COORD. Valid range is 0 degrees to 360 degrees (optional, default
%   is 40 degrees).
%   -ALTITUDE: For geodetic or geomagnetic coordinates, the height in km
%   above the Earth's surface. For geocentric coordinates, the radius in km
%   from the center of the Earth. Valid range for altitude is 0 km to 1000
%   km (optional, default when all other inputs are scalars is to sweep
%   from 0:50:1000 km and when any other input is an array is 100 km).
%   -UTC: Set to true (or 'UTC', 'U') if the times in TIME are in
%   Coordinated Universal Time (UTC) or false (or 'Local', 'LT', 'L') if
%   the times in TIME are in local time (optional, default is true).
%   -COORD: String specifying the coordinate system to use. Can be
%   geodetic ('geodetic', 'geod', or 'gd'), geomagnetic ('geomagnetic',
%   'geom', or 'gm'), or geocentric ('geocentric', 'geom', or 'gm')
%   (optional, default is geodetic).
%   -CURLDIR: Directory where curl.exe can be found (optional, only
%   necessary for Windows computers, and default for those is the same
%   directory that this function is located).
%   -F_10_7_DAILY: F_10.7 daily index to use in the model. Valid range is 0
%   to 400 (optional, default is to leave this field blank, in which case
%   it is taken from "real data base" [sic]).
%   -F_10_7_3MONTH: F_10.7 3 month average index to use in the model. Valid
%   range is 50 to 350 (optional, default is to leave this field blank, in
%   which case it is taken from "real data base" [sic]).
%   -AP_DAILY: Daily Ap index to use in the model. Valid range is 0 to 40
%   (optional, default is to leave this field blank, in which case it is
%   taken from "real data base" [sic]).
%
% Outputs:
%   -DENSITY: Array with each column having the following:
%       1. O: Atomic oxygen (O) number density in m^-3.
%       2. N2: Molecular nitrogen (N_2) number density in m^-3.
%       3. O2: Molecular oxygen (O_2) number density in m^-3.
%       4. MASS_DENSITY: Total mas density in kg/m^3.
%       5. HE: Atomic helium (He) number density in m^-3.
%       6. AR: Atomic argon (Ar) number density in m^-3.
%       7. H: Atomic hydrogen (H) number density in m^-3.
%       8. N: Atomic nitrogen (N) number density in m^-3.
%   -TEMPERATURE: Array with each column having the following:
%       1. TN: Neutrals temperature in K.
%       2. TEX: Exospheric temperature in K.
%   -F10_7_USED: Array with each column having the following:
%       1. F10.7 daily index used in the model.
%       2. F10.7 3 month average index used in the model.
%   -AP_USED: Array with each column having the following:
%       1. Daily Ap index used in the model.
%       2. Ap index used in the model from 0 to 3 hours prior.
%       3. Ap index used in the model from 3 to 6 hours prior.
%       4. Ap index used in the model from 6 to 9 hours prior.
%       5. Ap index used in the model from 9 to 12 hours prior.
%       6. Ap index used in the model from 12 to 33 hours prior.
%       7. Ap index used in the model from 33 to 59 hours prior.
```

```
%
% See also: MSISTEST, IRI, IGRF, DATENUM.

% Directory of this function.
fpath = mfilename('fullpath');
fpath = fpath(1:end-length(mfilename));

% Default behavior.
if nargin < 1 || isempty(time)
    time = datenum([2000 1 1 1 30 0]);
end
if nargin < 2 || isempty(latitude)
    latitude = 55;
end
if nargin < 3 || isempty(longitude)
    longitude = 45;
end
if nargin < 4 || isempty(altitude)
    if (ischar(time) || numel(time) == 1) && ...
            numel(latitude) == 1 && numel(longitude) == 1
        altitude = 0:50:1000;
    else
        altitude = 100;
    end
end
if nargin < 5 || isempty(utc)
    utc = true;
elseif ischar(utc)
    switch lower(utc)
        case {'utc', 'u'}
            utc = true;
        case {'local', 'lt', 'l'}
            utc = false;
        otherwise
            error('msis:badUTC', ['Unrecognized command ' utc '. Valid' ...
                ' options are ''utc'', ''u'', ''local'', ''lt'', or ' ...
                '''l''.']);
    end
end
if nargin < 6 || isempty(coord)
    coord = 'geod';
end
if isunix || ismac  % Curl is built-in to operating system.
    curldir = [];
elseif nargin < 7 || isempty(curldir)
    curldir = fpath;
end
if nargin < 8
    f_10_7_daily = [];
end
if nargin < 9
    f_10_7_3month = [];
end
if nargin < 10
    ap_daily = [];
end

% Convert time to a datenumber if it is a string.
if ischar(time)
    time = datenum(time);
```

```
end

% Convert the coordinates.
switch lower(coord)
    case {'geodetic', 'geod', 'gd'}
        geo_flag = '0.';
    case {'geocentric', 'geoc', 'gc'}
        % Convert coordinates to geodetic. The function ecef2geod assumes
        % meters, but we want km here.
        [x, y, z] = sph2cart(longitude*pi/180, latitude*pi/180, ...
            altitude*1e3);
        [latitude, longitude, altitude] = ecef2geod(x, y, z);
        altitude = altitude/1e3;
        geo_flag = '0.';
    case {'geomagnetic', 'geom', 'gm'}
        geo_flag = '1.';
    otherwise
        error('iri:coordCommandUnknown', ['Command ' coord ' unknown. ' ...
            'Valid options are ''geodetic'', ''geocentric'', and ' ...
            '''geomagnetic''.']);
end

% Error checking and input coversion.
if any(latitude < -90) || any(latitude > 90)
    error('msis:invalidLatitude', ['Input LATITUDE must be between ' ...
        '-90 degrees and 90 degrees.']);
end
longitude = mod(longitude, 360);
if any(altitude < 0) || any(altitude > 1e3)
    error('msis:invalidAltitude', ['Input ALTITUDE must be between ' ...
        '0 km and 1000 km.']);
end
if isempty(f_10_7_daily) || (f_10_7_daily >= 0 && f_10_7_daily <= 400)
    f_10_7_daily = sprintf('&f10_7=%#g', f_10_7_daily);
else
    error('msis:invalidF10_7_daily', ['Input F10_7_DAILY is %g but ' ...
        'must be between 0 and 400.'], f_10_7_daily);
end
if isempty(f_10_7_3month) || (f_10_7_3month >= 50 && f_10_7_3month <= 350)
    f_10_7_3month = sprintf('&f10_7_3=%#g', f_10_7_3month);
else
    error('msis:invalidF10_7_3month', ['Input F10_7_3MONTH is %g but ' ...
        'must be between 50 and 350.'], f_10_7_3month);
end
if isempty(ap_daily) || (ap_daily >= 0 && ap_daily <= 40)
    ap_daily = sprintf('&ap=%#g', ap_daily);
else
    error('iri:invalidTec_hmax', ['Input TEC_HMAX is %g km but must ' ...
        'be between 50 km and 2000 km.'], ap_daily);
end

% End of the string to be input into the system function.
endcmd = [f_10_7_daily f_10_7_3month ap_daily ...
    sprintf('&vars=%i', [5, 8:26]) ...
    '" https://ccmc.gsfc.nasa.gov/cgi-bin/modelweb/models/vitmo_model.cgi >
"' ...
    ...'"                                   https://ccmc.gsfc.nasa.gov/cgi-
bin/modelweb/models/vitmo_model.cgi > "' ...
    fullfile(fpath, 'temp.html"')];
```

```
% Get year, month, day, hour for MSIS.
[year, month, day, hour, minute, second] = datevec(time);
hour = hour + minute/60 + second/3600;
dayyear = dayofyear(year, month, day);

% Get the beginning of the string to be input into the system function.
if isunix || ismac % Curl is built-in to operating system.
    initialcmd = 'curl -k -d "model=msis';
else % Use the input curldir (possibly the default for that input).
    initialcmd = ['"' fullfile(curldir, 'curl"') ' -k -d "model=msis'];
end

% If one of the inputs can be swept keeping the others constant, run a
% sweep on the model.
A = [numel(unique(altitude)), numel(unique(latitude)), ...
    numel(unique(longitude)), numel(unique(year)), ...
    numel(unique(dayyear)), numel(unique(hour))];
if all(A == [1 1 1 1 1 1]) % Just one unique input.
    profile = 0;
elseif all(A == [A(1) 1 1 1 1 1]) % Sweep altitude.
    [sweep, tmp, sortind] = unique(altitude);
    if all(diff(diff(sweep)) < 1e-12)
        profile = 1;
        altitude = sweep(1);
        sweepmax = 1000;
    else % Altitude is unsweepable because steps are not linear.
        profile = 9;
    end
elseif all(A == [1 A(2) 1 1 1 1]) % Sweep latitude.
    [sweep, tmp, sortind] = unique(latitude);
    if all(diff(diff(sweep)) < 1e-12)
        profile = 2;
        latitude = sweep(1);
        sweepmax = 90;
    else % Latitude is unsweepable because steps are not linear.
        profile = 9;
    end
elseif all(A == [1 1 A(3) 1 1 1]) % Sweep longitude.
    [sweep, tmp, sortind] = unique(longitude);
    % Online interface can only have 100 km for longitude sweeps!
    if all(diff(diff(sweep)) < 1e-12) && altitude == 100
        profile = 3;
        longitude = sweep(3);
        sweepmax = 360;
    else % Longitude is unsweepable because steps are not linear.
        profile = 9;
    end
elseif all(A == [1 1 1 A(4) 1 1]) % Sweep year.
    [sweep, tmp, sortind] = unique(year);
    if all(diff(diff(sweep)) < 1e-12)
        profile = 4;
        year = sweep(1);
        sweepmax = 2012;
    else % Year is unsweepable because steps are not linear.
        profile = 9;
    end
elseif all(A == [1 1 1 1 A(5) 1]) % Sweep day of year or month.
    [sweep, tmp, sortind] = unique(dayyear);
    if all(diff(diff(sweep)) < 1e-12)
        profile = 7;
```

```
        dayyear = sweep(1);
        sweepmax = 366;
    % Day of year steps are not linear, but maybe month steps are.
    elseif numel(day(1)) == 1
        [sweep, tmp, sortind] = unique(month);
        profile = 5;
        month = sweep(1);
        sweepmax = 12;
    else % Day of year is unsweepable because steps are not linear.
        profile = 9;
    end
elseif all(A == [1 1 1 1 1 A(6)]) % Sweep hour in a day.
    [sweep, tmp, sortind] = unique(hour);
    if all(diff(diff(sweep)) < 1e-12)
        profile = 8;
        hour = sweep(1);
        sweepmax = 24;
    else % Hour is unsweepable because steps are not linear.
        profile = 9;
    end
else
    profile = 9;
end

% Call curl depending on the sweep profile.
switch profile
    case 0
        [status, result] = system([initialcmd ...
            sprintf('&year=%i', year) ...
            sprintf('&month=%i', month) ...
            sprintf('&day=%i', day) ...
            sprintf('&time_flag=%i', ~utc) ...
            sprintf('&hour=%#g', hour) ...
            '&geo_flag=' geo_flag ...
            sprintf('&latitude=%#g', latitude) ...
            sprintf('&longitude=%#g', longitude) ...
            sprintf('&height=%#g', altitude) ...
            '&profile=1' ...
            sprintf('&start=%#g', altitude) ...
            sprintf('&stop=%#g', altitude) ...
            '&step=1.' ...
            endcmd]);
        if status == 0
            data = parseresult(fpath, 1);
        else
            error('msis:curlError', ['Curl command did not work. ' ...
                'It returned status:%i, ' regexprep(result, '\\', ...
                '\\\\')], status);
        end
    case {1 2 3 4 5 7 8}
        % The online interface will only output up to a sweep length of
        % 500, so split the sweep into increments of 500.
        nsweeps = ceil(numel(sweep) / 500);
        sweepstart = sweep(1 : 500 : end);
        sweepstop = [sweep(500 : 500 : end), sweep(end)];
        sweepstep = mode(diff(sweep));
        sweeplen = round((sweepstop - sweepstart) ./ sweepstep + 1);
        prevsweeplen = [0 sweeplen(1:end-1)];
        sweepstop = min([sweep(end) + sweepstep/10, sweepmax]);
        data = zeros(20*sum(sweeplen), 1);
```

```
        for index = 1:nsweeps
            [status, result] = system([initialcmd ...
                sprintf('&year=%i', year(1)) ...
                sprintf('&month=%i', month(1)) ...
                sprintf('&day=%i', day(1)) ...
                sprintf('&time_flag=%i', ~utc) ...
                sprintf('&hour=%#g', hour(1)) ...
                '&geo_flag=' geo_flag ...
                sprintf('&latitude=%#g', latitude(1)) ...
                sprintf('&longitude=%#g', longitude(1)) ...
                sprintf('&height=%#g', altitude(1)) ...
                sprintf('&profile=%i', profile) ...
                sprintf('&start=%#g', sweepstart(index)) ...
                sprintf('&stop=%#g', sweepstop) ...
                sprintf('&step=%#g', sweepstep) ...
                endcmd]);
            if status == 0
                data((1:20*sweeplen(index)) + 20*prevsweeplen(index)*...
                    (index-1)) = parseresult(fpath, sweeplen(index));
            else
                error('msis:curlError', ['Curl command did not work. ' ...
                    'It returned status:%i, ' ...
                    regexprep(result, '\\', '\\\\')], status);
            end
        end
    % profile = 9 means there is more than one unique run to make. Turn all
    % the scalars into vectors with the same number of elements as the
    % largest array. If there is an array smaller than the largest array,
    % throw an error.
    case 9
        maxnum = max([numel(altitude), numel(latitude), ...
            numel(longitude), numel(year), numel(day), numel(month), ...
            numel(hour)]);
        if numel(altitude) == 1
            altitude = repmat(altitude, maxnum, 1);
        elseif numel(altitude) ~= maxnum && numel(altitude) > 1
            error('msis:invalidSize', ['Input vectors must all have ' ...
                'the same number of elements.']);
        end
        if numel(latitude) == 1
            latitude = repmat(latitude, maxnum, 1);
        elseif numel(latitude) ~= maxnum && numel(latitude) > 1
            error('msis:invalidSize', ['Input vectors must all have ' ...
                'the same number of elements.']);
        end
        if numel(longitude) == 1
            longitude = repmat(longitude, maxnum, 1);
        elseif numel(longitude) ~= maxnum && numel(longitude) > 1
            error('msis:invalidSize', ['Input vectors must all have ' ...
                'the same number of elements.']);
        end
        if numel(time) == 1
            year = repmat(year, maxnum, 1);
            month = repmat(month, maxnum, 1);
            day = repmat(day, maxnum, 1);
            hour = repmat(hour, maxnum, 1);
        elseif numel(time) ~= maxnum && numel(time) > 1
            error('msis:invalidSize', ['Input vectors must all have ' ...
                'the same number of elements.']);
        end
```

```
        data = zeros(20*maxnum, 1);
        for index = 1:maxnum
            [status, result] = system([initialcmd ...
                sprintf('&year=%i', year(index)) ...
                sprintf('&month=%i', month(index)) ...
                sprintf('&day=%i', day(index)) ...
                sprintf('&time_flag=%i', ~utc) ...
                sprintf('&hour=%#g', hour(index)) ...
                '&geo_flag=' geo_flag ...
                sprintf('&latitude=%#g', latitude(index)) ...
                sprintf('&longitude=%#g', longitude(index)) ...
                sprintf('&height=%#g', altitude(index)) ...
                '&profile=1' ...
                sprintf('&start=%#g', altitude(index)) ...
                sprintf('&stop=%#g', altitude(index)) ...
                '&step=1.' ...
                endcmd]);
            if status == 0
                data((1:20) + 20*(index-1)) = parseresult(fpath, 1);
            else
                error('msis:curlError', ['Curl command did not work. ' ...
                    'It returned status:%i, ' regexprep(result, '\\', ...
                    '\\\\')], status);
            end
        end
end % End case

% data has all the data in one long vector and consists of 1 independent
% variable (height) and 19 dependent variables (the various outputs of the
% function). Therefore, a particular variable's data occurs in steps of 20
% in data. The model outputs height even though we don't care about it
% because otherwise it doesn't work in some cases.
O = data(2:20:end);
N2 = data(3:20:end);
O2 = data(4:20:end);
mass_density = data(5:20:end);
Tn = data(6:20:end);
Tex = data(7:20:end);
He = data(8:20:end);
Ar = data(9:20:end);
H = data(10:20:end);
N = data(11:20:end);
f_10_7_daily_used = data(12:20:end);
f_10_7_3month_used = data(13:20:end);
Ap_daily_used = data(14:20:end);
Ap_00_03 = data(15:20:end);
Ap_03_06 = data(16:20:end);
Ap_06_09 = data(17:20:end);
Ap_09_12 = data(18:20:end);
Ap_12_33 = data(19:20:end);
Ap_33_59 = data(20:20:end);

% Resort the output if we did a sweep.
if profile >= 1 && profile <= 7
    O = O(sortind);
    N2 = N2(sortind);
    O2 = O2(sortind);
    mass_density = mass_density(sortind);
    Tn = Tn(sortind);
    Tex = Tex(sortind);
```

```
    He = He(sortind);
    Ar = Ar(sortind);
    H = H(sortind);
    N = N(sortind);
    f_10_7_daily_used = f_10_7_daily_used(sortind);
    f_10_7_3month_used = f_10_7_3month_used(sortind);
    Ap_daily_used = Ap_daily_used(sortind);
    Ap_00_03 = Ap_00_03(sortind);
    Ap_03_06 = Ap_03_06(sortind);
    Ap_06_09 = Ap_06_09(sortind);
    Ap_09_12 = Ap_09_12(sortind);
    Ap_12_33 = Ap_12_33(sortind);
    Ap_33_59 = Ap_33_59(sortind);
end

% Output.
density = [O, N2, O2, mass_density./1e3, He, Ar, H, N] .* 1e6;
temperature = [Tn, Tex];
f_10_7_used = [f_10_7_daily_used, f_10_7_3month_used];
Ap_used = [Ap_daily_used, Ap_00_03, Ap_03_06, Ap_06_09, Ap_09_12, ...
    Ap_12_33, Ap_33_59];


% Return the day of the year.
function dayyear = dayofyear(year, month, day)

previous = cumsum([0, 31, 28, 31, 30, 31, 30, 31, 31, 30, 31, 30]);
dayyear = previous(month) + day + double( ...
    (~mod(year, 4) & mod(year, 100)) | (~mod(year, 400)) & (month > 2) );


% Parse the result file output by the system command.
function data = parseresult(fpath, sweeplen)

% Get the data from the file temp.html into a string, then delete the file.
fid = fopen(fullfile(fpath, 'temp.html'), 'r');
if fid == -1
    error('msis:parseresult:cannotOpenFile', ['Cannot open temp.html ' ...
        'file generated by curl command.']);
end
result = fread(fid, '*char').';
f = fclose(fid);
if f == -1
    warning('msis:parseresult:cannotCloseFile', ['Cannot close ' ...
        'temp.html file generated by curl command.']);
end
delete(fullfile(fpath, 'temp.html'));

% Data starts at line 37. If there isn't a line 37, there was an error.
newlines = find(result == sprintf('\n'));
if length(newlines) < 201
    % Output the error with the HTML tags removed.
    error('msis:parseresult:modelWebError', regexprep(['The online ' ...
        'interface returned:\n' result], '<[^>]*>', ''));
end

data = sscanf(result(newlines(200)+1 : newlines(200 + sweeplen)-1), '%f');
```